PALAIOS
Emphasizing the impact of life on Earth's history

PALAIOS, 2023, v. 38, 188–209
Research Article
DOI: http://dx.doi.org/10.2110/palo.2022.020

# SIMPLE STRUCTURES AND COMPLEX STORIES: POTENTIAL MICROBIALLY INDUCED SEDIMENTARY STRUCTURES IN THE EDIACARAN SERRA DE SANTA HELENA FORMATION, BAMBUÍ GROUP, EASTERN BRAZIL

JULIANA OKUBO,[1] LUCAS INGLEZ,[1] GABRIEL J. UHLEIN,[2] LUCAS V. WARREN,[1] AND SHUHAI XIAO[3]
[1]*Department of Geology, São Paulo State University, Rio Claro 13506-900, Brazil*
[2]*Federal University of Minas Gerais, CPMTC-IGC, Belo Horizonte, 31270-901 MG, Brazil*
[3]*Department of Geosciences, Virginia Tech, Blacksburg, Virginia 24061, USA*
*email: juliana.okubo@unesp.br*

**ABSTRACT: Microbially induced sedimentary structures (MISS) are abundant in Ediacaran and lower Cambrian successions. However, the relationship between MISS distribution and facies has not been thoroughly explored in Ediacaran–Cambrian successions in South America. This study documents the occurrence of MISS and other potential biogenic structures from the late Ediacaran Serra de Santa Helena Formation in the Bambuí Group of eastern Brazil. This unit overlies the *Cloudina*-bearing Sete Lagoas Formation and is a mixed carbonate-siliciclastic succession devoid of macroscopic body fossils. Potential microbial structures include wrinkled structures such as "elephant-skin" and Kinneyia-like textures, as well as pustular structures and abundant positive epirelief discoidal structures. Another putative biogenic structure is a mm-wide meandering groove resembling a simple locomotion trail of a small vagile benthic metazoan. Microbial surface textures (i.e., "elephant skin" and Kinneyia-type wrinkles) were mainly observed in heterolithic deposits, usually at the interface between sandstone and siltstone/shale. On the other hand, discs show a facies-independent distribution, observed in heterolithic as well as carbonate and marl deposits. Petrographic analyses of these discs suggest that they have complex origins and some of them may be diagenetic structures. Thus, while facies may have strongly controlled the preservation of MISS-related structures and textures in the Serra de Santa Helena Formation, their abundance and diversity in tidal flat deposits indicate the wide distribution of matgrounds in these shallow marine paleoenvironments. Also, we demonstrate how detailed description and classification of simple features, such as discoidal structures, is an important task for paleoenvironmental reconstruction of marine ecosystems at the Ediacaran–Cambrian transition when the microbially bounded substrates played important roles in the dynamics of coastal environments.**

## INTRODUCTION

During much of the Proterozoic Eon, low to intermediate energy shallow marine sediments were sealed by an extensive cover of microbial mats and biofilms (Bouougri and Porada 2002; Noffke et al. 2002). In siliciclastic settings, these matgrounds conditioned the development of a whole class of biosedimentary structures, collectively known as MISS (microbially induced sedimentary structures, *sensu* Noffke et al. 1996). Due to the influence of viscous microbial substances such as extracellular polymeric substances (EPS), MISS often develop and preserve intricate wrinkled patterns such as Kinneyia, "Old Elephant Skin" and arumberiamorph textures (Hagadorn and Bottjer 1997; Gehling and Droser 2009; Kolesnikov et al. 2012, 2017; Kumar and Ahmad 2014). In addition, other sedimentological features might be important indicators of microbial activity in ancient environments, including but not limited to: (1) microbial gas entrapping structures or gas domes (Bosak et al. 2010; Mata et al. 2012; Knoll et al. 2013); (2) discoidal structures (Gerdes et al. 2000; Hagadorn and Miller 2011; Taj et al. 2014; Menon et al. 2016; Inglez et al. 2022); (3) "sand chips" (Pflüger and Gresse 1996; Bouougri and Porada 2002); (4) sinusoidal cracks (Bouougri and Porada 2002); (5) multidirectional ripple marks (Noffke 1998); and (6) erosional remnants and pockets (Noffke 1999).

In late Ediacaran and early Cambrian, benthic motile metazoans interacted with matgrounds and exploited them for food and possibly oxygen, disturbing the substrate and/or ingesting mat-laden sediment (Buatois and Mángano 2011b; Gingras et al. 2011; Buatois et al. 2014; Mángano and Buatois 2016; Xiao et al. 2019). In this context, microbial related structures may be associated with the preservation of trace fossils and other delicate biological structures (Hagadorn and Bottjer 1999; Bouougri and Porada 2007; Porada and Bouougri 2008; Buatois et al. 2014; Meyer et al. 2014; O'Neil et al. 2020; Droser et al. 2022), making the identification and interpretation of MISS and related features a key task to understand their paleoecological relationships, sedimentary processes, biogenicity, and spatial and temporal distribution.

Discoidal structures are also very common in Ediacaran strata and usually associated with microbially related structures (Luo et al. 2016; Menon et al. 2016; Bykova et al. 2017; Bobrovskiy et al. 2018; Inglez et al. 2019, 2022; Ye et al. 2020). However, the interpretation of these morphologically simple structures should be taken with caution as they can represent either abiotic- or biotic structures (Inglez et al. 2019). Depending on their shape, size, and relief, simple discoidal structures have been interpreted as body and trace fossils of various affinities, ranging from microbial colonies (Grazhdankin and Gerdes 2007), to macroalgae (Wang et al. 2017), to holdfast structures of sessile organisms (e.g., form genus *Aspidella*, Gehling et al. 2000). Also, several simple plug-shaped structures, attributed to resting or shallow dwelling burrows (e.g., *Bergaueria* and *Conichnus*) can be preserved as discoidal features on

Published Online: April 2023
 0883-1351/23/038-188

the bedding plane (Pemberton et al. 1988; McIlroy et al. 2005). Finally, discoidal structures can be generated through abiotic processes, such as concretion formation (Anderson et al. 2016; Schwid et al. 2021) and fluid escape (Menon et al. 2016; Inglez et al. 2022).

In the Brazilian Precambrian record, microbial structures have been described in many sedimentary basins, including different types of stromatolites and associated structures (Dardenne and Campos Neto 1975; Souza and Müller 1984; Zaine 1991; Sallun Filho and Fairchild 2000; Nogueira et al. 2003; Zucatti Da Rosa 2005; Warren et al. 2014; Fairchild and Sanchez 2015; Romero et al. 2016). The most studied Neoproterozoic unit from South America is undoubtedly the Bambuí Group in eastern Brazil. Numerous studies on the sedimentology, stratigraphy, geochemistry, and geochronology of the Bambuí provide a robust geologic background for this unit (e.g., Dardenne 1978; Vieira et al. 2007; Alvarenga et al. 2014; Paula-Santos et al. 2015, 2017; Caxito et al. 2018; Okubo et al. 2018; Caetano-Filho et al. 2019; Uhlein et al. 2019; Guacaneme et al. 2021). However, despite its likely Ediacaran–Cambrian age (Warren et al. 2014; Moreira et al. 2020; Tavares et al. 2020), the scarcity of definitive Ediacaran–Cambrian fossils is notable (Dardenne and Campos Neto 1975; Fairchild et al. 1996; Fairchild and Sanchez 2015; Fairchild and Subacius 1986; Sanchez et al. 2018, 2021; Warren et al. 2014). In particular, macrofossils are extremely rare in the Bambuí Group. These are restricted to a few localized occurrences of parautochthonous skeletal remains of *Cloudina* sp. and putative *Corumbella werneri* fragments (Warren et al. 2014). Recently, an occurrence of putative trace fossils identified as *Treptichnus pedum* in association with MISS has been described in the Três Marias Formation, the uppermost unit of the Bambuí Group (Sanchez et al. 2021). Microbial structures are less conspicuous and generally poorly preserved in predominantly siliciclastic units of the Bambuí Group (Sanchez et al. 2018; Santos et al. 2018; Uhlein et al. 2020), hampering their identification and interpretation.

In this contribution, we present several types of microbially related structures from the mixed carbonate-siliciclastic platform of the Serra de Santa Helena Formation, characterized by an extremely positive carbon isotope anomaly (Middle Bambuí Excursion or MIBE; Uhlein et al. 2019) and one of the less-studied units in the Bambuí Group. The presence of MISS, discoidal and pustular structures, and possible simple trails shed new light on the paleontological content of this unit that was previously considered barren of paleobiological data. The presence of distinct microbial mat-related structures within certain carbonate and siliciclastic facies is analyzed, aiming at elucidating the relationship between sediment substrates and microbial communities.

## GEOLOGICAL BACKGROUND

The São Francisco Craton (SFC) in central Brazil consists of an Archean–Paleoproterozoic igneous and metamorphic basement covered by Meso- and Neoproterozoic mixed siliciclastic-carbonate sequences. The Bambuí Group represents a late Neoproterozoic to early Cambrian succession deposited directly above the basement or overlying the Paleo- to Mesoproterozoic metasedimentary units (Fig. 1A). It comprises six formal lithostratigraphic units (Dardenne 1978) that include, in ascending order: (1) the Jequitaí Formation (diamictite, conglomerate, sandstone, and shale); (2) the Sete Lagoas Formation (limestone and dolostone); (3) the Serra de Santa Helena Formation (limestone, siltstone and marl); (4) the Lagoa do Jacaré Formation (dark limestone and shale); (5) the Serra da Saudade Formation (green siltstone, shale, sandstone and limestone), and (6) the Três Marias Formation (arkose, conglomerate, and shale) (Fig. 1B).

The basal Sete Lagoas Formation corresponds to a post-Marinoan cap carbonate, followed by laminated and cross-laminated grainstone, laminated microbialite, mudstone, thrombolite with skeletal remains of *Cloudina* sp. and simple trace fossils (Santos et al. 2004; Vieira et al. 2007; Warren et al. 2014; Kuchenbecker et al. 2016; Perrella et al. 2017). The upper part of this unit comprises trough-cross bedded ooid grainstone, breccia, and pseudo-columnar and domal stromatolites (Okubo et al. 2020).

The Serra de Santa Helena Formation stands between the carbonate-dominated Sete Lagoas and Lagoa do Jacaré formations, and it was interpreted as a transgressive succession related to a basin-wide drowning event (Dardenne 1978). In many places, including the Januária and Montalvânia regions in the northern Minas Gerais state (Fig. 1A), the Serra de Santa Helena Formation encompasses about 200 m thick siltstone and shale, with sparse occurrences of carbonate, marl, and tabular beds of fine sandstone (Uhlein et al. 2019). The lower part of the succession is composed of thinly laminated rhythmite (siltstone and shale), microbial carbonates, and marl, followed by matrix-rich and fine-grained arkose, commonly presenting heterolithic bedding. Toward the top of the Serra de Santa Helena succession, black to gray, pyrite-rich rhythmite with rare intercalations of marl and microbialite become progressively common (Iglesias and Uhlein 2009; Uhlein et al. 2019). Microbialite beds and associated carbonates yield $\delta^{13}C$ values characteristic of the Middle Bambuí Excursion (MIBE) interval, ranging from +7.3 to +12.5‰ VPDB (Uhlein et al. 2019). The presence of mixed carbonate-siliciclastic facies with local evidence of subaerial exposure (e.g., mudcracks) and salt pseudomorphs indicates deposition in inter- to supratidal settings under transitory evaporitic conditions (Uhlein et al. 2019). Domal and columnar stromatolites, as well as laminated microbialites, have also been described in the overlying Lagoa do Jacaré Formation (Iglesias and Uhlein 2009; Fragoso et al. 2011; Santos et al. 2018; Uhlein et al. 2019).

The depositional age of the Bambuí Group has been intensely debated in the past few decades. The basal Sete Lagoas cap dolostone has been interpreted as early Ediacaran based on the presence of aragonite and barite fans, negative $\delta^{13}C$ values, and anomalous $\Delta^{17}O$ values characteristic of Ediacaran cap dolostone elsewhere around the world (Caxito et al. 2012; Crockford et al. 2018; Okubo et al. 2018). The middle Sete Lagoas Formation is substantially younger, because it contains the terminal Ediacaran index fossil *Cloudina* (550–538 Ma; Warren et al. 2014) and a population of detrital zircon grains with ages of ~ 557 Ma (Paula-Santos et al. 2015). More recently, novel *in-situ* carbonate U-Pb dating provided strong evidence for a hiatus between the lower and middle Sete Lagoas Formation (Caxito et al. 2021). Geochronologic (and/or biostratigraphic) data constraining the age of the Serra de Santa Helena and Lagoa do Jacaré formations are rare. But U-Pb dating of volcanic zircon grains from a tuff layer of the Serra da Saudade Formation yielded an age of 520.2 ± 5.3 Ma, suggesting an early Cambrian age for the upper part of the Bambuí Group (Fig. 1B; Moreira et al. 2020). Thus, the stratigraphic interval from the *Cloudina*-bearing level in the middle Sete Lagoas Formation to the Serra da Saudade Formation represents at least 35 Myr of depositional history from the late Ediacaran to the early Cambrian.

From the upper Sete Lagoas Formation to the lower Serra da Saudade Formation, the Bambuí Group presents carbonate rocks showing anomalously high $\delta^{13}C$ values (up to +16‰ VPDB) as part of the MIBE (Uhlein et al. 2019). The origin of the MIBE is still enigmatic, but Cui et al. (2020) emphasized its regional nature and argued for water-column methanogenesis and subsequent release of $^{13}C$-depleted methane to the atmosphere as the main driver of $^{13}C$ enrichment of the water column in a restricted basin (Caetano-Filho et al. 2020; Cui et al. 2020).

## MATERIAL AND METHODS

Due to the poor exposure and limited outcrops, this study is focused on two sections of the middle–upper Serra de Santa Helena Formation at Pitarana (14°22′47.16″S, 44°23′1.52″W) and Lontra areas (15°42′53.21″S, 44°23′20.43″W) in the northern Minas Gerais state (Fig. 1C, 1D). Detailed stratigraphic sections (1:50) were logged at both localities. Sedimentary facies were characterized in the field and samples

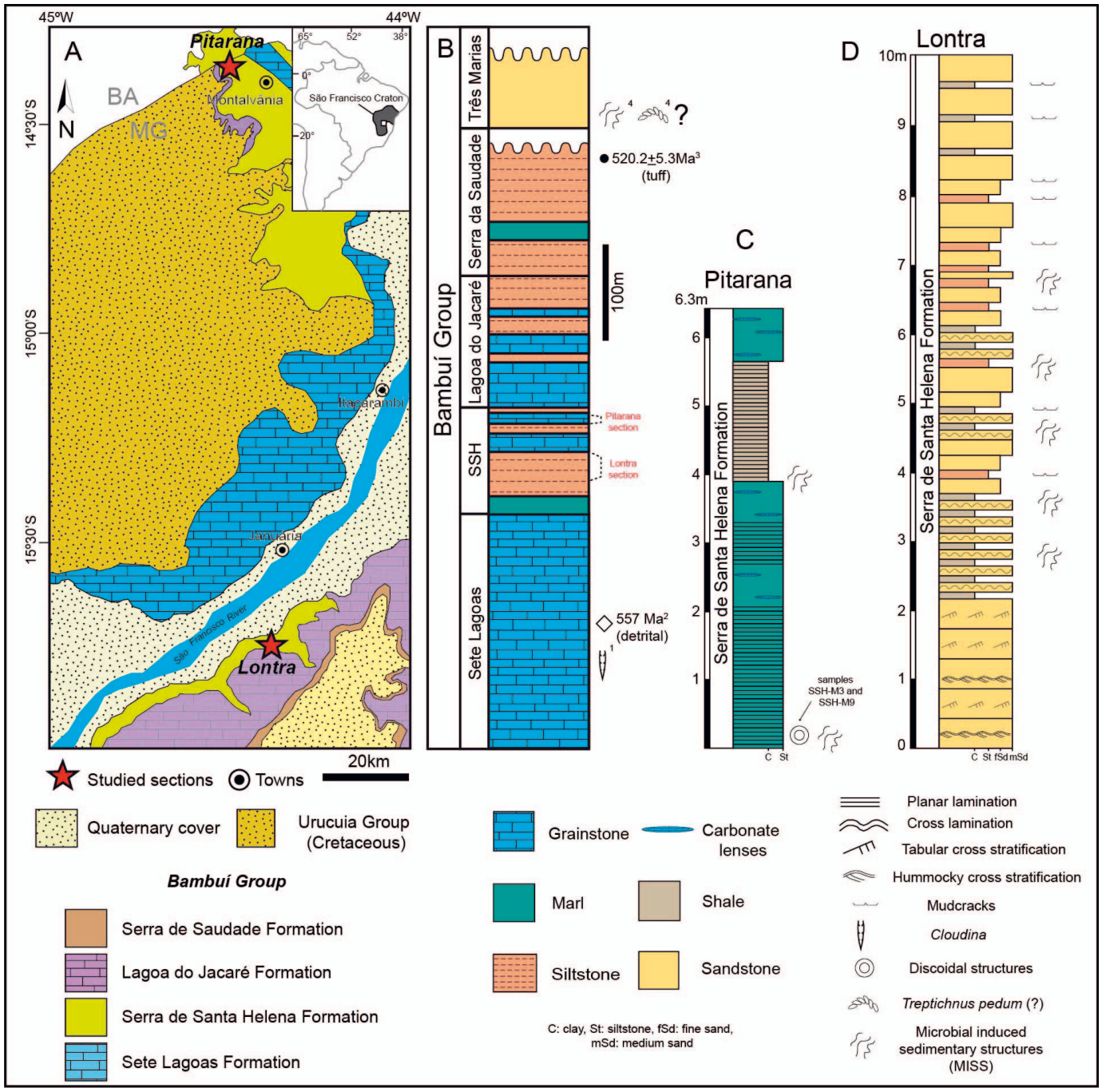


FIG. 1.—Geology of the study area in central-eastern Brazil. **A**) Simplified geological map of the studied area, showing the two measured stratigraphic sections (Pitarana and Lontra localities, red stars). **B**) Generalized lithostratigraphic column of the Bambuí Group in the Januária area. The approximate stratigraphic intervals of logged sections at the Pitarana and Lontra are marked. **C**, **D**) Logged stratigraphic sections at Pitarana (C) and Lontra (D), showing sedimentary facies and stratigraphic distribution of MISS and discoidal structures described in this work. Paleontological and geochronological data are from: (1) Paula-Santos et al. (2015); (2) Warren et al. (2014); (3) Moreira et al. (2020), and (4) Sanchez et al. (2021). Key: BA = Bahia State; MG = Minas Gerais State; SSH = Serra de Santa Helena Formation.

containing MISS, discs, and other putative biotic structures were collected from both localities. Several samples were collected as floats, and the following criteria were used to infer stratigraphic orientation or the probable top bedding surface of the float samples: (1) the infill of sand cracks, which seems to represent passive infill with material from above; (2) the association of sand-cracks with sand-infilled domes, which likely represent plastic deformation features derived from the accumulation of fluids beneath a cohesive layer (i.e., gas-domes), and (3) the presence of discs described below as type 4 discs, with depressed rims and elevated central regions, which seem to represent the counterparts of collapsed domes. The presence of these features in float samples allowed us to infer original stratigraphic orientations. As imperfect as this approach may be,

our observations give coherent results and are consistent with previously published material of modern and fossil MISS (Porada and Bouougri 2007).

The samples were observed under a stereoscopic microscope and photographed with a Nikon-D3100 digital camera and a camera arm Kaiser RTX. Selected samples were sectioned perpendicular to the bedding plane and polished with carborundum abrasive on a manual grinder. Polished slabs were scanned on a high-resolution digital scanner (1600 dpi). Petrographic analysis of polished thin sections was conducted on a transmitted light microscope, allowing for the characterization of sedimentary grains and sedimentary structures that formed the basis for microfacies interpretation.

The samples containing discoidal structures (type 1, SSH-M3 and type 2, SSH-M9) and Type 2 wrinkle structures (SSH-1) were also examined under an epifluorescence microscope using UV light to assess the presence of organic matter. Additionally, Raman analysis was performed in the EMU LabRam Laboratory, São Carlos Institute of Physics, University of São Paulo (Brazil), on a Raman Spectroscopy System (Horiba LabRam HR Evolution UV-VIS-NIR). Excitation was provided by a 532 nm laser focused onto the sample through a 100× objective. The target for Raman analysis was carbonaceous material in the same samples analyzed by epifluorescence.

After epifluorescence microscopy and Raman spectroscopy analyses, samples of discoidal structures were carbon-coated for electron probe analysis (EPMA) with energy dispersive X-ray spectroscopy (EDS) and X-ray wavelength dispersive spectroscopy (WDS). The analysis was performed at the Department of Geology, São Paulo State University, Brazil, on a JEOL JXA 8230 superprobe equipped with 5 WDS spectrometers and a panchromatic cathodoluminescence system (XM-26730PCL). Elemental and cathodoluminescence maps were acquired at accelerating voltage of 15keV and probe current of 20 nA in order to identify major elements: Si (Kα), Al (Kα), Ca (Kα), Mg (Kα), Fe (Kα), and K (Kα).

The distinct surface textures described in Serra de Santa Helena Formation (Table 1) were categorized following the protocol of Davies et al. (2016), indicating the degree of confidence on the biogenicity of the structures. The descriptions were systematized in two groups, Category A (abiotic) and Category B (biotic/microbial). Additionally, Category Ba was assigned for structures with evidence for biotic origin, but an abiotic origin cannot be ruled out; and Category Ab was for the opposite situation. Surface textures with a plausible biotic origin, but without clear evidence, are classified as category ab. The analyzed specimens are housed at the Department of Geology, São Paulo State University, Rio Claro Campus, São Paulo, Brazil, and identified by their respective numbers in the figure captions.

Fresh carbonate samples were selected for carbon and oxygen isotope analysis. Powders were micro-drilled from discoidal structures (Type 1 discs) and the surrounding matrix, avoiding fractures and veins. Aliquots of the powders were allowed to react with 100% $H_3PO_4$ under He atmospheric conditions. Carbon and oxygen isotopic compositions of extracted $CO_2$ were then measured in a Delta V Advantage mass spectrometer at the LAMIR, Federal University of Paraná, Brazil. Isotopic results are reported in the conventional delta notation ($\delta^{13}C_{carb}$ and $\delta^{18}O_{carb}$) as per-mil deviation from the Vienna Pee Dee Belemnite (VPDB).

## RESULTS

### *Sedimentary Facies*

The Pitarana section (Figs. 1C, 2A, 2B) is a 6.5 m-thick succession in the upper Serra de Santa Helena Formation, predominantly composed of cm-to-dm thick tabular beds of laminated marl, sometimes interbedded with carbonate lenses and black shale. In the middle–upper part of the section, there occurs a ~ 1.6 m-thick interval of rhythmically alternating beds of siliciclastic siltstone and shale. Discoidal structures occur exclusively in the lower part of the measured section, occasionally associated with wrinkle structures. Despite the limited outcrop available for study and the monotonous variation of lithotypes (Fig. 1C), it can be inferred that the facies association represents deposition by settling in relatively calm waters, probably below the fair-weather wave base in a mixed carbonate-siliciclastic ramp.

The Lontra section is a 10 m-thick succession of the middle Serra de Santa Helena Formation (Fig. 1D). It begins with tabular medium-grained cross-bedded sandstone interbedded with rare hummocky and swaley cross-stratified fine sandstone. In the middle part of the measured section, medium- to fine-grained quartz sandstone is interbedded with yellowish to reddish laminated siltstone. Beds of wave-rippled sandstone (Fig. 2C), fine siltstone, and shale often show heterolithic bedding and mud cracks (Fig. 2D), and a variety of wrinkled and pustular textures (Fig. 3) occur in this interval. Near the top of the measured section, tabular beds of immature sandstone are interbedded with shale where abundant mud cracks are found.

Sedimentary structures at the Lontra section suggest deposition in a tidally influenced setting in which cross-bedded sandstone deposited in subtidal channels grades into heterolithic facies in intertidal settings. Fine-grained facies with mud cracks are interpreted as muddy deposits of inter- to supratidal flats, subjected to periodical subaerial exposure (Fig. 1D). Thus, the siliciclastic facies from the Lontra succession were interpreted to have been deposited in shallower conditions than the marl and rhythmite from the Pitarana succession. Overall, the general stacking pattern suggests a deepening succession for the middle to the upper part of the Serra de Santa Helena Formation in the study area (see Uhlein et al. 2019 for further explanations).

### *Sedimentary Surface Textures*

**Wrinkle Structures and Associated Textures.**—Wrinkled surfaces are the most common type of sedimentary surface textures observed on the bedding planes in the lower and middle parts of the Pitarana section and in the middle part of the Lontra section. They are found in heterolithic deposits, marked by the intercalation of cm-scale, fine to very fine sandstone layers, and mm-scale, discontinuous siltstone laminae, with occasional mudstone intraclasts.

Wrinkle structures were observed either at the top (epirelief) or bottom (hyporelief) of beds and can be generally divided into three distinct morphological categories. Type 1 wrinkles are mostly observed on the rippled or planar surface of fine sandstone beds and are characterized by millimeter-scale, densely distributed pits and flat-topped domes (Figs. 2C, 3A–3C), resembling "honeycomb texture" pattern (Hagadorn and Bottjer 1999; Porada and Bouougri 2007). Type 2 is recognized on an undulated surface at the top of very fine, centimeter-thick sandstone beds and is marked by sub-centimetric bulges and depressions, sometimes with a slightly aligned pattern (Fig. 3D–3F). Type 3 occurs either as epi- and hyporelief features, associated with thin veneers of micaceous siltstone. This type of wrinkle structures is best preserved at the bottom of beds and is characterized by a very delicate crinkled texture, with sub- to millimeter-size bulges and grooves (Fig. 4A–4C), or occasionally aligned patterns (Fig. 4D–4F). At the upper bedding surface, this pattern is marked by delicate ridges, separated by submillimeter-scale, near-circular depressions. Co-occurrence of Types 2 and 3 was observed on intercalated surfaces within heterolithic beds.

In cross-section, beds bearing Type 1 wrinkles do not show any prominent features and are characterized by well-sorted, very fine sandstone mostly composed of angular grains of quartz. However, slabs of heterolithic beds show that Type 2 texture is often marked by disrupted

TABLE 1.—*Microbially induced sedimentary structures of the Serra de Santa Helena Formation, Bambuí Group.*

| Structure type | Description | Interpretation |
|---|---|---|
| Wrinkle structures (Ba or B) | *Type 1*–Millimeter-scale, densely distributed pits and flat-topped domes (Figs. 2C, 2D, 3A–3C), resembling a "honeycomb texture" pattern. They are preserved at flat or rippled bed surface of fine-grained sandstone. | Small-scale load casts forming pitted pattern resulted from biostabilization of sandy substrates by endobenthic mats |
| | *Type 2*—Sub-centimetric bulges and depressions, sometimes distributed with a slightly aligned pattern as seen on top of an undulate surface on the top of very fine cm-thick sandstone bedding planes (Fig. 3D). In cross section, they present well-defined borders and pronounced convex tops and flat bottoms (Fig. 3E), occasionally marked by disrupted and flexibly deformed lamination. At the micrometer-scale, lamination is characterized by a well-defined crinkling pattern (Fig. 5A), often showing cuspate or flame-like geometry (Fig. 5A, 5B). Quartz grains are mostly angular and randomly oriented, while platy phyllosilicate grains are predominantly oriented parallel to bedding, often following the crinkly laminated structures (Fig. 5C). | Small-scale load casts forming pitted pattern with occasional sand cracks resulted from biostabilization of sandy substrates by endobenthic mats |
| | *Type 3*—Millimetric to submillimetric bulges and grooves distributed at the top of micaceous siltstone beds with a reticulate (Fig. 4A–4C), or sometimes aligned pattern (Fig. 4D and E). Also observed as submillimetric epirelief ridges and near-circular depressions at the bottom of beds. The Type 3 wrinkle structures are marked by delicate crinkled texture in cross section. | Reticulate pattern associated with the colonization of the surface by epibenthic mats |
| Pustular and discoidal structures (A or Ab) | *Type 1*—Subcircular or slightly elongate to irregularly shaped epirelief mounds preserved within a 3-5 mm thick light-colored carbonate bed, intercalated with dark, thinly laminated mudstone/marl deposit. Mounds range from 6 to 10 mm in diameter, and are preserved as solitary or clustered individuals with mutually deformed margins (Fig. 6A). These structures are 0.37 mm high (mean vertical relief). Locally marked by a slight central depression. In cross section, no clear lateral boundary is observed between the discs and the light-colored bed in which they occur (Figs. 6B–6D). The lower surface of this bed is often undulated, showing symmetric crests and throughs (Fig. 6B). The light-colored bed is composed of carbonate matrix with scattered opaque minerals. Opaque minerals are also common in the discs-bearing bed, interpreted as partially oxidized framboidal pyrite crystals (Fig. 7C–7E). | Selective cementation of the disc-bearing beds during early diagenesis |
| | *Type 2*—Isolated or clustered epirelief domes (Fig. 8A and B) or hyporelief depressions (Fig. 8C) in marl facies. They range from 4 to 9 mm in diameter (mean diameter of 5 mm), and 0.1 mm high (mean vertical relief, n = 88). Domes are infilled with light-colored calcite microspar, greatly contrasting with the dark-gray mudstone sediment above and below (Fig. 8D–8H). They are observed both as discrete (Fig. 8D) or laterally connected individuals in cross section (Fig. 8E). Locally, laminae above and below the discs are deformed (Fig. 8D and E). Small patches of pyrite crystals occur near the margin of the discoidal structures (Fig. 8G, 8H). Carbonaceous material is detected both within the discoidal structures and in underlying bed (Fig. 9C, 9E). | Entrapment and accumulation of fluids produced by the decay of the buried mat underneath a cohesive microbial mat surface. These discoidal structures are somewhat similar to *Intrites* and *Nimbia* (Menon et al. 2016; Néraudeau et al. 2018) |
| | *Type 3*—Circular or semi-circular features preserved in marl facies as positive epirelief discs. They are marked by pronounced raised margins and depressed central regions forming either a "C" or "Donut"-shaped structures ranging from 0.8 to 1 cm in diameter (Fig. 11A). Inner depressions show a mean diameter of 0.45 mm. Usually observed as isolated structures, they occasionally form clusters of up to 2 or 3 individuals. Clustered discs can be coalesced or mutually deformed. | |
| | *Type 4*—Elliptical structures with a mean diameter of 0.4 cm (ranging from 0.3 to 0.5 cm), showing slightly raised margins and a wide flat central area (Fig. 11B). Discs are preserved as epirelief features in top of fine-grained sandstone beds, occurring either isolated or connected with each other, forming a chain-like pattern with their long axes aligned (Fig. 11C). Vertical cross sections do not reveal any structure in depth. | |
| Simple trail (Ba or B) | Elongate, rectilinear to curved negative epirelief groove flanked by raised margins (levees) at one terminal end (Fig. 11D) in a fine-grained sandstone. Preserved in the same bed as the Type 4 ellipsoidal structures, both linear groove and the elongation axes of discs are approximately parallel to the throughs of ripple marks. | Possible interpretations include sinusoidal cracks analogous to "*Manchuriophycus*", the probable pseudo trace fossil *Vaqueiroichnus stewarti* (McMenamin 2016) or a simple trail within the morphological spectrum of *Helminthopsis-Archaeonassa* |

and plastically deformed lamination. Type 2 wrinkling pattern at the surface of these beds is marked by a laterally continuous lamina of fine-grained sediment, presenting crinkly and wavy aspects. Under the microscope, thin sections containing Type 2 texture show millimeter-scale layers of clean quartz silt or well-sorted, very fine to fine-grained quartz sand interbedded with thin layers of dark-colored mud (Fig. 5A–5C). The dark muddy layers are brownish in color under epifluorescence microscopy (Fig. 5D). Raman analysis of the dark muddy layers was compromised by their fluorescent nature, possibly due to the presence of clay minerals. The micrometer-scale lamination of the dark layers is characterized by a well-defined crinkling pattern (Fig. 5A), often showing cuspate or flame-like microstructures (Fig. 5A, 5B). Quartz grains are mostly angular and are randomly oriented. Platy phyllosilicate minerals are predominantly oriented parallel to bedding, sometimes following the crinkly laminated structures observed in thin sections (Fig. 5C).

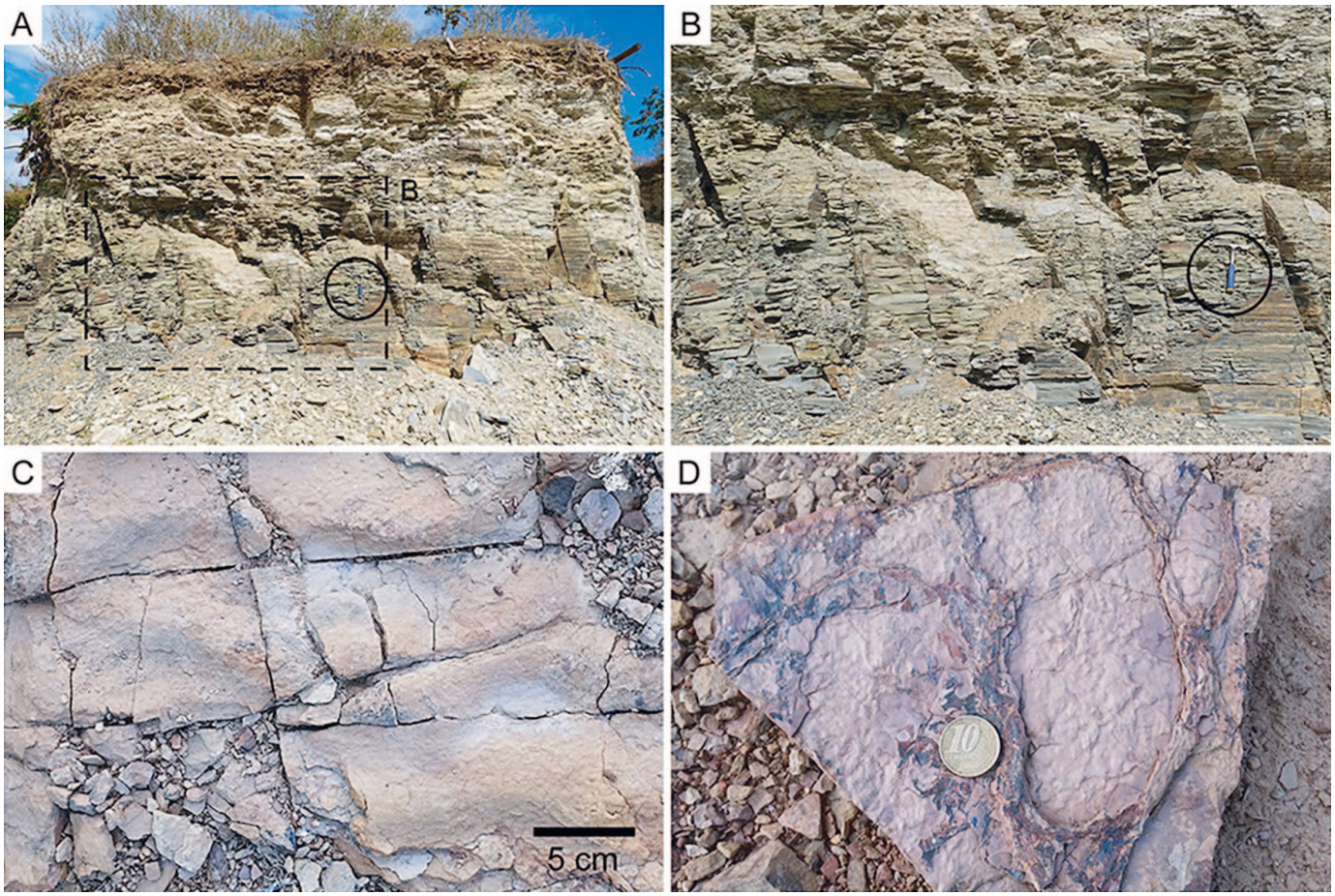


FIG. 2.—Field photographs of the Pitarana section and sedimentary structures of the Lontra section. **A**) Studied outcrop of the Serra de Santa Helena Formation at the Pitarana section. **B**) Detail of A showing interbedded massive and laminated marl. **C**) Ripple marks in fine sandstone at the Lontra section. Top bedding surface view. **D**) Siltstone with polygonal mud cracks and wrinkled pattern at the Lontra section. Bottom bedding surface view. Rock hammer (A, B) is 25 cm long and coin (D) is 2 cm in diameter.

**Discoidal Structures.**—Discoidal structures are abundant at several levels of the studied interval and were identified in different facies associations (cross-laminated fine sandstone, laminated siltstone, and marl) at both sections. The described structures show considerable morphological and size variations and can be classified into four distinct categories (Types 1–4; Figs. 6–10, 11A–11C). Type 1 discoidal structures are subcircular to elongate to irregularly shaped mounds preserved on the top surface (positive epirelief) of a thin (~ 2 mm) light-colored carbonate bed intercalated with dark, thinly laminated mudstone/marl layers, in the lower part of the Pitarana section (sample SSH-M3; Figs. 1C, 6A). They range from 6 to 10 mm in diameter, occurring either as solitary structures or in clusters containing up to three individual protrusions. Occasionally, there is either a slight depression or a protuberance in the central part of the structure. Closely packed mounds are often deformed near their touching margins, and some larger, irregularly shaped structures seem to have resulted from the merging of two or more individual discs (Fig. 6A). Under the microscope, the lower surface of the disc-bearing bed is smooth and undulate, showing symmetric crests and troughs in profile (Fig. 6B) and the discs have a vertical relief of 0.37 mm (range = 0.26–0.45 mm, n = 6). Carbonate carbon isotope compositions are similar between the disc-bearing bed ($\delta^{13}C_{carb}$ = +5.9 ‰ VPDB) and the underlying dark-colored sediment ($\delta^{13}C_{carb}$ = +5.3 ‰ VPDB; Fig. 6B).

There are no clear boundaries between the discoidal structures (Fig. 6B–6E); in fact, the discoidal structures form a continuous bed that is underlain and overlain by dark-colored matrix (Fig. 6B–6D). The disc-bearing bed is composed of light-colored carbonate sediments and cement, with disseminated opaque minerals (Figs. 6B–6D, 7A, 7C). No epifluorescence was identified within these discoidal structures or in the matrix (Fig. 7A, 7B). The opaque minerals in the disc-bearing bed occur as small reddish sub-spherical aggregates, ranging from 10 to 20 μm in diameter (Fig. 7C–7E). They probably represent scattered iron oxide/hydroxide pseudomorphs after the oxidation of framboidal pyrite, based on the distribution of Fe (Fig. 7D–7F). Back-scattered images and EDS data reveal euhedral pyrite and iron oxide, with residual pyrite dispersed in a matrix composed of calcite and scattered quartz grains (Fig. 7E, 7F).

Cathodoluminescence and elemental maps do not show any boundary between the disc-bearing bed and the infilling of the mounds, and both seems to be composed of homogeneous calcite cement with microspar morphology. Immediately overlying the discs there is a thin lamina, which is enriched in Si, Al, Fe, and Mg, indicating the presence of clay minerals (Figs. 6E, 7B, 7F).

Type 2 discoidal structures are relatively small subcircular domes that range from 4 to 9 mm in diameter (n = 88, mean diameter of 5 mm) and typically have a central depression (Fig. 8A–8C). They are preserved as either positive epirelief (Fig. 8B) or negative hyporelief (Fig. 8C), with a vertical relief of 0.1 mm (range = 0.09–0.16 mm, n = 16). Although the discs are often isolated from each other, they may form localized clusters, with closely spaced domes showing deformed margins and poorly defined boundaries (Fig. 8B), similarly to those observed in Type 1 discs (Fig. 6A).

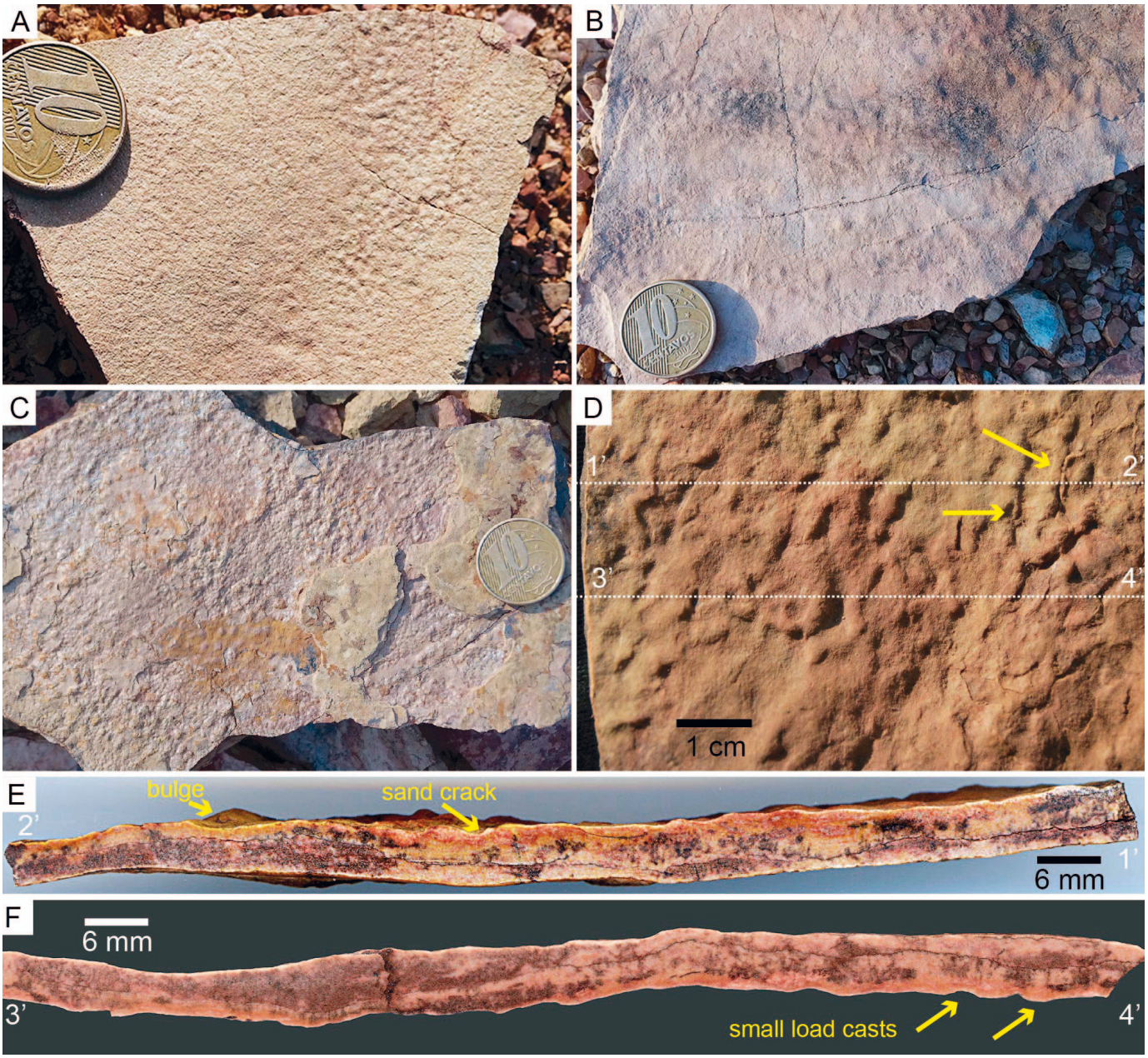


FIG. 3.—Wrinkle structures in the Serra de Santa Helena Formation. **A**–**C**) 'Honeycomb' texture (Type 1) in very fine sandstone (A, B) and coarse siltstone (C) from the Lontra section. All are floats but probably top bedding surface views. **D**) Sub-centimetric bulges and depressions, sometimes with a slightly aligned pattern associated with mm-scale sand cracks (Type 2). Yellow arrows indicate sand cracks. Float but probably top bedding surface view. **E**) Cross-section of D (section 1′–2′) showing bulges and surficial sand cracks. **F**) Cross-section of D (section 3′–4′) showing small-scale load structures (yellow arrows). Coin (A–C) is 2 cm in diameter.

Interestingly, these disc-bearing surfaces are marked by a distinct positive-relief reticulate to irregularly shaped pattern that seems to connect the discs. The discs have a greater positive relief than the reticulate pattern (Fig. 8B). In cross-section, most individual domes show a flat lower surface with a sharply defined boundary (Fig. 8D–8F), which separates the discs from underlying sediment (Fig. 8G, 8H). One slab sectioned perpendicular to the bedding plane revealed lensoidal structures (Fig. 8E, white arrow) that are similar in composition to the discoidal structures exposed on the slab upper surface (Fig. 8E, yellow arrows). However, these lensoidal structures have a flat top and a convex-downward bottom (Fig. 10C, 10D). Domes are infilled with light-colored calcite microspar, which greatly contrasts with the sediment above and below (Figs. 8D, 8F–8H, 9A, 9C–9D). This sediment consists of gray mudstone layers rich in scattered sand and silt-sized quartz and mica grains, which are interbedded with black organic-rich laminae (sample SSH-M9, Fig. 8D, 8F, 8G). No vertical tubular structures or convex down lenses were observed within the discs (Fig. 8D, 8E, 8F), but there are some fractures cutting the infilling vertically (Fig. 9D). No epifluorescence was identified within these discoidal structures or in the matrix (Fig. 9A, 9B). However, Raman spectroscopic analysis shows that carbonaceous material is present in both the discoidal structure and underlying layer (Fig. 9C, 9E).

Elemental maps show that the matrix is enriched in Mg, Si, Al, and K, whereas the disc is homogeneous and Ca-rich (Fig. 10E). In other words, the disc is predominantly calcitic in composition with some silicate

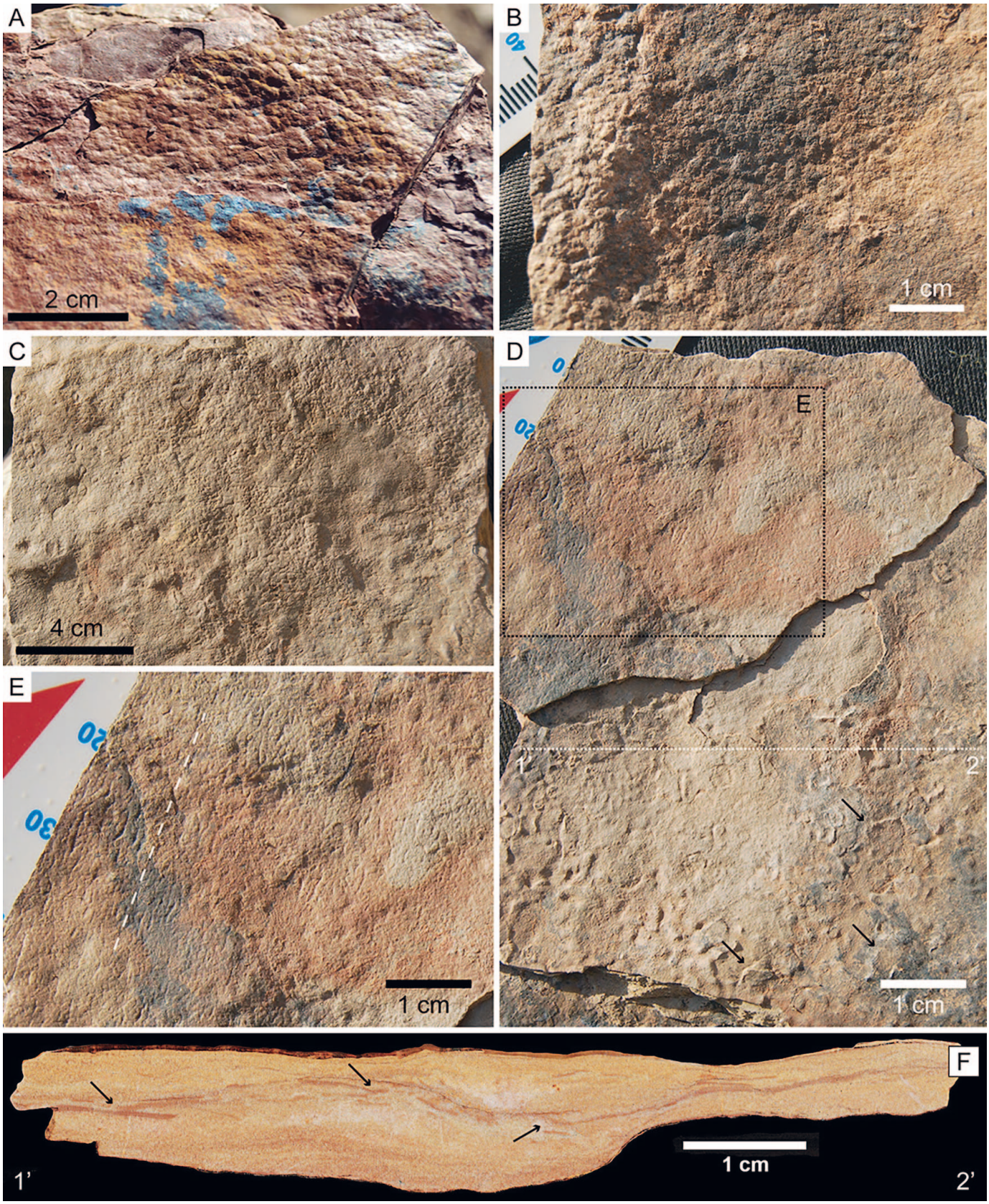


FIG. 4.—Type 3 wrinkles in siliciclastic facies of the Serra de Santa Helena Formation. **A**–**C**) 'Elephant-skin' texture in siltstone (A) and fine-grained sandstone (B, C) from the Lontra section. All are floats but probably top bedding surface views. **D**) Millimetric ridges and grooves preserved in fine-grained sandstone at the Lontra section. Note mat chips in lower right (black arrows). Float but probably top bedding surface view. **E**) Detail of D showing Arumberia-like structure. Parallel alignment of grooves is denoted by white dashed line. **F**) Cross-section of D (1′–2′) showing disrupted laminae (black arrows) of fine-grained sediment overlain by sandstone. Float but upper surface probably represents top bedding surface.

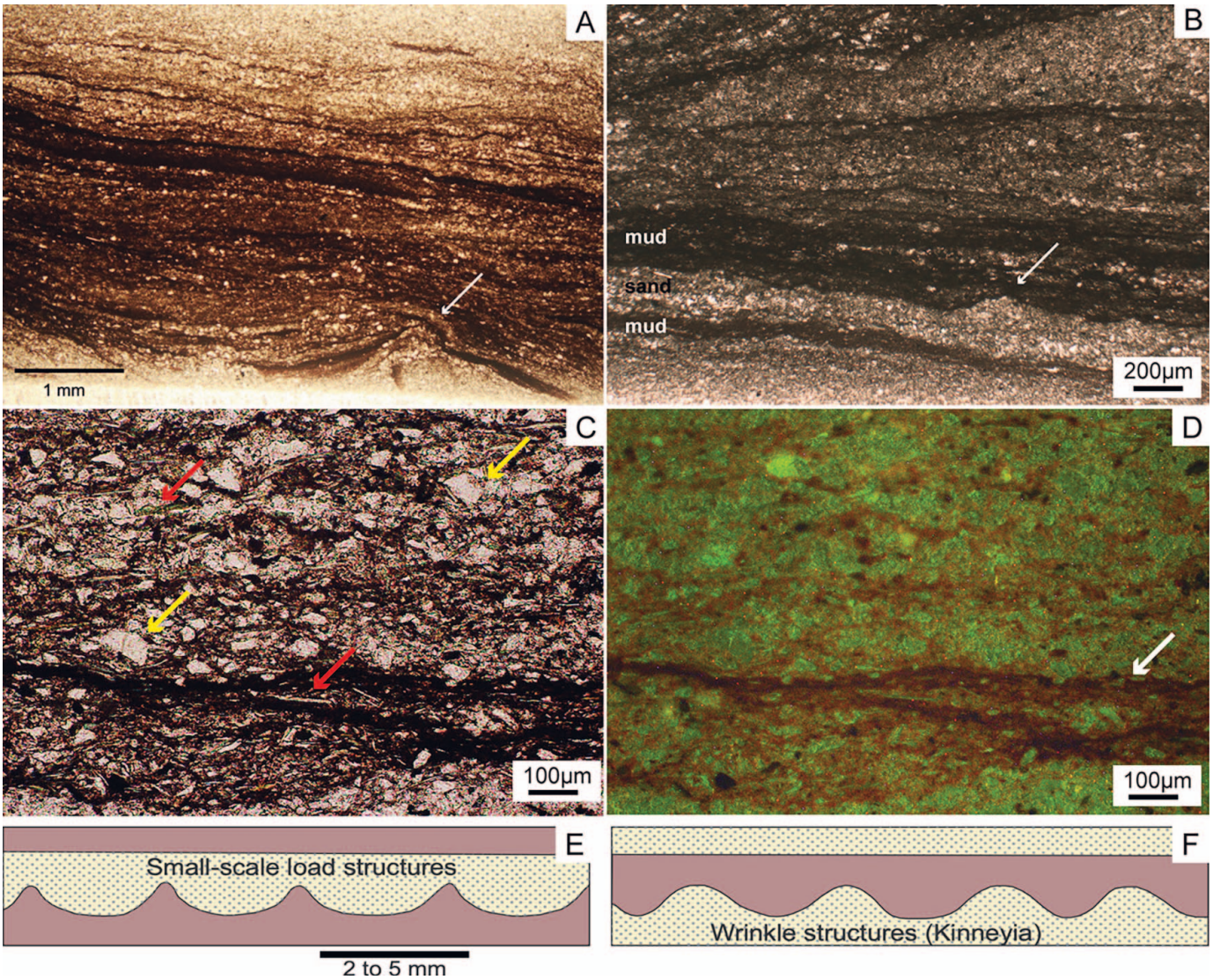


FIG. 5.—Petrographic thin-section photomicrographs under parallel polarized light and interpretive diagrams of Type 2 wrinkle structures from siliciclastic facies of the Serra de Santa Helena Formation at the Lontra section. **A**) Fine-grained sandstone preserving crenulated/crinkled microlaminae, showing cuspate or flame-like microstructures (white arrow). Stratigraphic up-direction unknown. **B**) Section transverse to wrinkle structures showing several mud-sand-mud triplets and a cuspate or flame-like microstructures (white arrow). **C**, **D**) Bright-field light microscopic image (C) and corresponding epifluorescence microscopic image (D) detailing the mud-sand-mud triplets. Yellow arrows in C mark quartz grains, which seems to be randomly oriented. Red arrows in C mark phyllosilicate minerals that are predominantly parallel to the bedding. In D, quartz grains in fine-grained sandstone show green epifluorescent color whereas microbial laminar are brownish in color (white arrow). **E**, **F**) Schematic comparison between small-scale load structures and wrinkle structures (Kinneyia), modified from Porada et al. (2008); (E) load structures with downward protrusions of sandstone (light yellow) or coarse siltstone (dots) into underlying mudstone (maroon). Individual loads are separated by sharp-crested ridges in underlying mudstone; (F) wrinkle structures (Kinneyia) with upward protrusions of sandstone or coarse siltstone into overlying siltstone or mudstone. Note the flat contact with overlying tabular bed (mudstone in E or sandstone in F).

minerals (as shown by the Si map) and the matrix is composed of dolomite, quartz, and phyllosilicates.

Type 3 discs show a donut or more rarely C-shaped morphology and occur on top of dark-colored marl beds (Fig. 11A). They are 0.8–1.0 cm in diameter and have a raised margin surrounding a central depression (~ 0.45 cm in diameter; Fig. 11A). They are usually found scattered on the bedding plane, but a dense aggregate is seen to occupy a localized area of 2 to 2.4 $cm^2$ (Fig. 11A, upper left). When aggregated, discs are observed to deform each other or coalesce into more irregular structures (Fig. 11A, upper left).

Finally, Type 4 discoidal structures were observed either at the top or at the bottom surface of very fine micaceous sandstone at the Lontra section.

→

FIG. 6.—Type 1 discoidal structures from the Serra de Santa Helena Formation at the Pitarana section. **A**) Discoidal structures on a top bedding plane. Note that some discs show a small irregular hollow at the center of structure. **B**) Cross-section of discoidal structures (dashed line in (A) showing persistent lateral continuity between discs. Carbon isotope values of a discoidal structure and underlying sedimentary matrix are marked on the figure. Stratigraphic up-direction on top. **C**, **D**) Parallel- (PPL) and cross-polarized (XPL) light microscopic images of B. **E**) Cathodoluminescence (CL) and elemental maps of area marked by rectangle in B, showing no prominent boundaries between discoidal structures. Elements are marked in lower left of each panel.

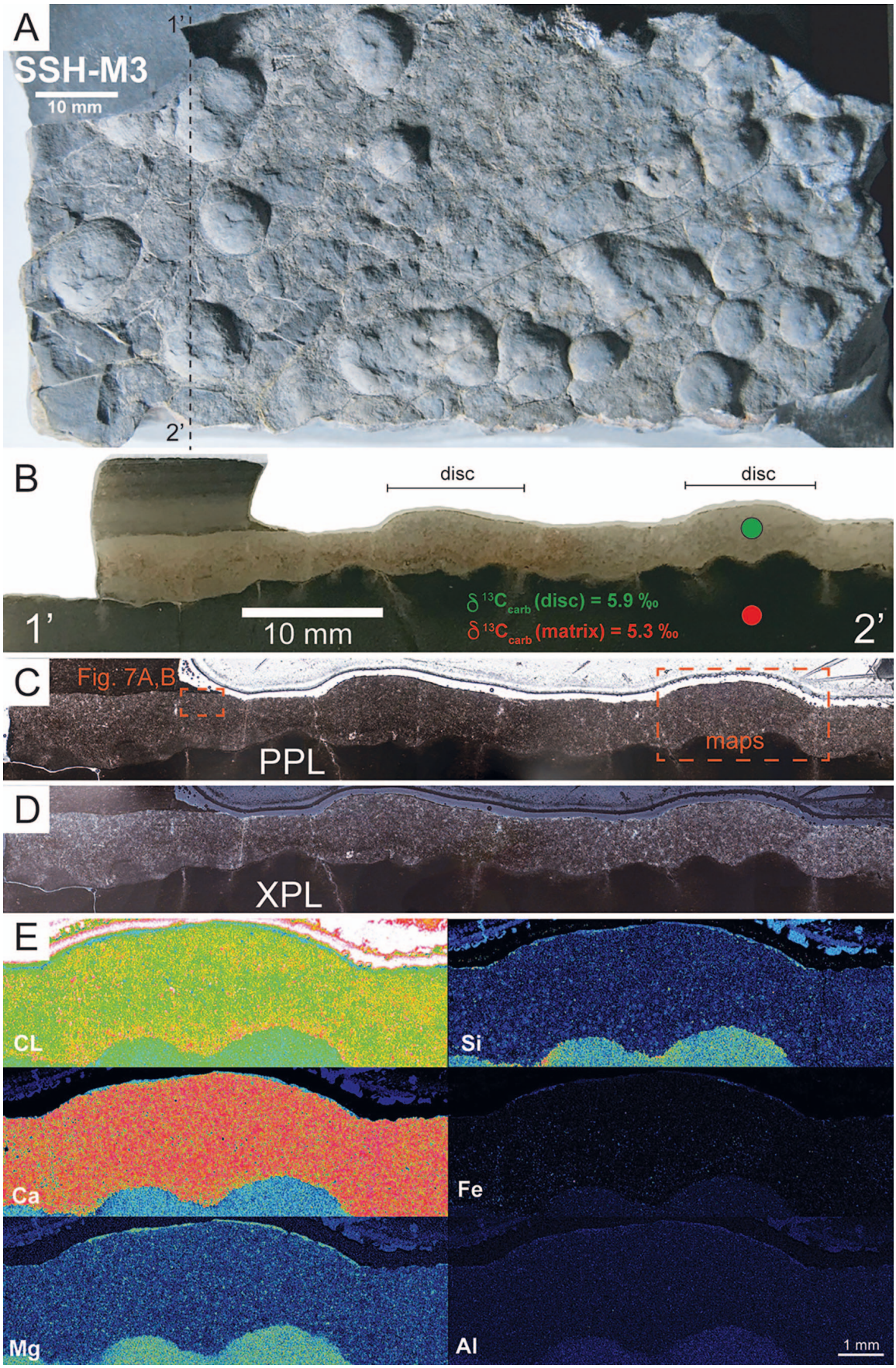

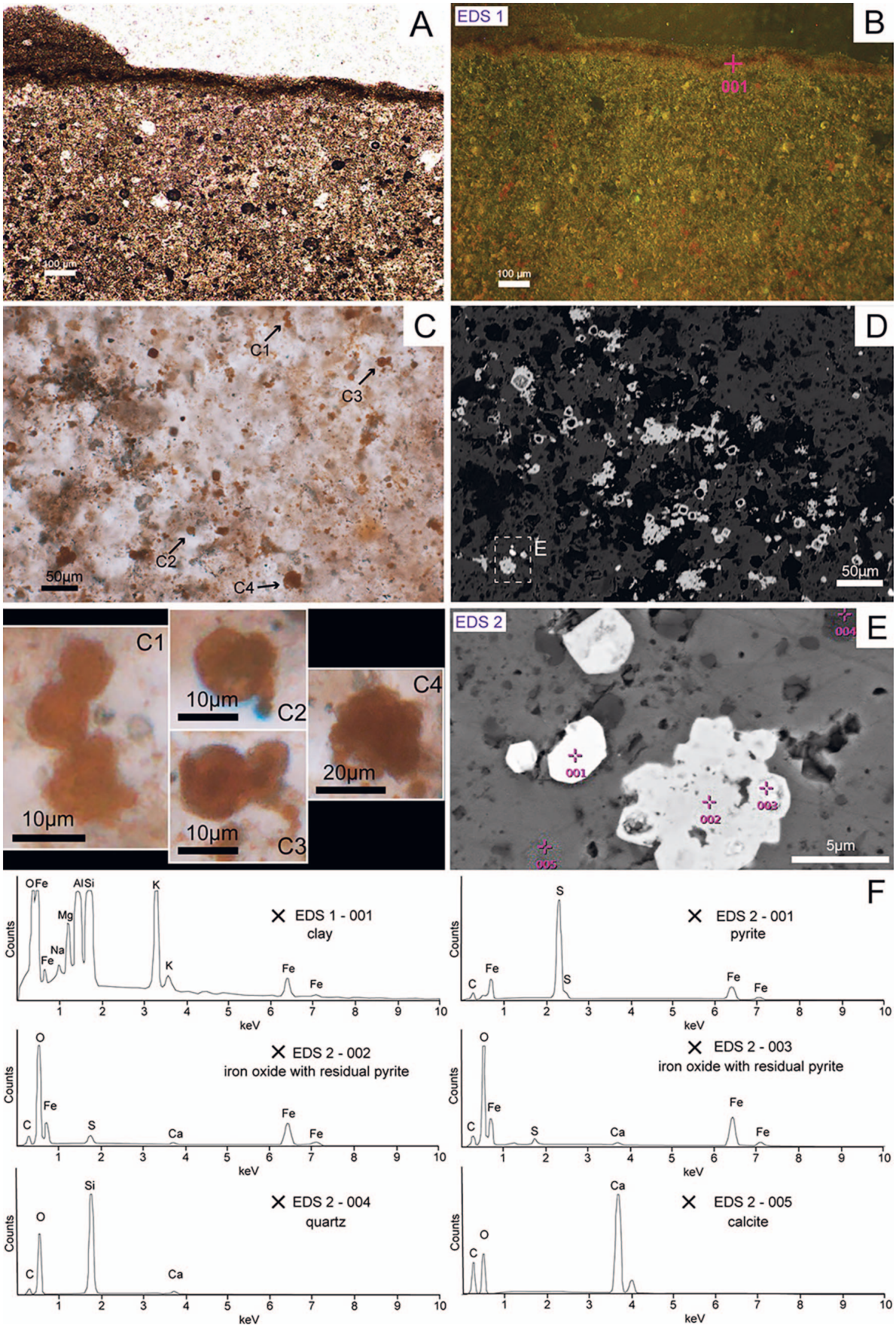

The discs range from 0.3 to 0.5 cm in diameter, and show a subcircular to elliptical morphology. In epirelief, they are characterized by a wide and flat central area surrounded by a relatively thin and raised margin. When observed in hyporelief, the margin is marked by a discrete subcircular groove. The discs are often coalesced with each other to form a chain-like feature (Fig. 11B, 11C). Cross-sections did not reveal any distinctive internal structures associated with this type of disc, which indicate that the discs and the matrix are both composed of very fine-grained sandstone.

**Meandering Groove as a Possible Trace Fossil.—**A poorly preserved curved to meandering groove (Fig. 11C–11D) is present on the top surface of a fine sandstone bed bearing ripple marks, wrinkle structures, and Type 4 discoidal structures. At one terminal part of the structure, the shallow groove is flanked by raised margins (Fig. 11D), resembling lateral levees and possibly indicating active sediment displacement. Interestingly, the slab illustrated in Figure 11C shows a slightly undulate surface with a pattern that may indicate former ripple marks partially levelled by the colonization of epibenthic mats (see Noffke et al. 2002 for similar examples). The groove structure and the elongation axes of ellipsoidal structures (Type 4 discs) are both oriented parallel to the troughs.

## DISCUSSION

Determining the biotic versus abiotic origin of bedding-surface textures is not an easy task (Hagadorn and Bottjer 1997, 1999; Thomas et al. 2013), although several criteria have been proposed (see Davies et al. 2016; Noffke 2009, 2018; Noffke et al. 2002, among others). One well-accepted protocol was originally proposed by Noffke (2009), who outlined diagnostic characteristics of MISS. According to Noffke (2009), (1) MISS must occur in sedimentary rocks that experienced no more than low-grade metamorphism; (2) MISS commonly occur at regression-transgression transition in stratigraphic sections; (3) microbial mats develop and become preserved under specific hydraulic and depositional conditions; (4) the distribution of MISS is not random, but it reflects the average hydraulic pattern in a defined area; (5) the geometries and dimensions of MISS must correspond to modern examples; and (6) MISS represent, were caused by, or are related to ancient biofilms or microbial mats, identified in thin sections as wavy crinkled laminae and filament-like textures, often in association with framboidal pyrite. Because abiotic processes may create patterns mimicking true MISS, the biotic versus abiotic interpretation of MISS-like structures should be built on multiple lines of evidence combining paleoenvironmental, lithological, macrostructural, textural, geochemical, and mineralogical data (Hagadorn and Bottjer 1997; Noffke 2009, 2021; Noffke et al. 2022).

According to Noffke et al. (2022), MISS are defined into five classes reflecting the dominant microbial activity that governs the formation of the structures: (1) structures caused by growth; (2) structures caused by biostabilization; (3) structures caused by baffling and trapping; (4) structures caused by binding; and (5) structures caused by the interference of all above-mentioned microbial activities.

### *Wrinkle Structures*

Interpretive classifications of microbially related textures, such as wrinkle marks, often take into consideration their taphonomic and ecological significance (Gerdes et al. 2000; Noffke 2018). Type 1 and Type 2 wrinkles are preserved on top of very fine sandstone and occasionally in sandstone intercalated with siltstone veneers (Fig. 3A–3D). They resemble patterns of honeycomb textures, which is sometimes considered within the morphological spectrum of Kinneyia-like structures (Porada and Bouougri 2007; Porada et al. 2008). These features have been considered as the record of small-scale load casts developed in sandstone and siltstone deposits due to rapid sediment deposition over a biostabilized substrate (Porada et al. 2008). Indeed, cuspate and flame-like structures of millimeter-scale were observed in vertical cross-sections of heterolithic beds containing Type 2 wrinkles (Fig. 5A, 5C). Also, small-scale surficial sand cracks can occur in association with these textures (Fig. 3D), and both features can be explained by the enhanced cohesiveness of these deposits due to sediment binding by endobenthic mats in higher energy settings within the intertidal zone. In modern environments, these shallow intrastratal communities can develop during latency periods of few hours associated with daily tide related hydrodynamic variations (Noffke 2010).

Microbial binding is controlled by sedimentary parameters and produces structures such as reticulate patterns with centimeter- to millimeter-scale ridges and tufts (Gerdes et al. 2000; Shepard and Sumner 2010). *In-situ* preservation of microbial mats requires a pause in sedimentation, during which the mat develops, and the deposition of fine-grained sediment that drapes the mat surface and replicates the mat fabrics (Noffke et al. 2022). These microbial-sedimentary processes likely contributed to the formation of Type 3 wrinkles, which are marked by greater morphological details and are characterized by reticulate patterns similar to elephant skin textures (Fig. 4A–4E). They occur in association with millimeter-scale laminae of siltstone and claystone within heterolithic deposits, probably representing the record of more mature epibenthic mats that developed during longer latency periods within the supratidal zone (Noffke 2010; Cuadrado et al. 2014).

←

FIG. 7.—Type 1 discoidal structures from the Serra de Santa Helena Formation at the Pitarana section. **A**, **B**) Close-up views of area marked by the left rectangle in Figure 6C. Bright-field light microscopic image (A) and corresponding epifluorescence microscopic image (B), showing the upper surface of the disc-bearing bed and the overlying thin lamina. **C**) Small reddish spherical structures dispersed in the calcite matrix (labeled arrows C1–C4, with magnifications in lower left panel), possibly representing oxidized pyrite framboids. **D**, **E**) Back-scattered (BSE) images of oxidized pyrite framboids, which have bright colors due to the presence of iron. Rectangle in D marks area shown in E; (E) Pyrite and iron oxide with residual pyrite in a calcitic matrix with some quartz grains. **F**) EDS spectra of areas marked in B and E, representing a clay layer overlying discoidal structures in B (EDS 1) and the presence of pyrite, iron oxide, calcite, and quartz in E (EDS 2).

→

FIG. 8.—Type 2 discoidal structures from the Serra de Santa Helena Formation at the Pitarana section. **A**) Top bedding surface view of marl, showing several cm-sized discs scattered in the bedding surface. **B**) Detail of Type 2 discoidal structures locally forming clusters (black arrow). Top bedding surface view. **C**) Bottom bedding surface view of negative hyporelief characterized by locally connected shallow impressions with central knobs or ridges. **D**) Cross-section showing the distribution of discoidal structures within the same bed. Discoidal structures have a convex-up top and a flat base, with overlying sediment layer warping around the discoidal structures. Stratigraphic up-direction on top. **E**) Vertically cut and polished slab showing two distinct disc-bearing beds, separated by alternating thin layers of dark- and light-colored sediments. The upper bed contains isolated discs with a convex-up top and a flat base (yellow arrows), whereas the lower bed contains discs with a flat top and convex-down base (white arrow). These two disc-bearing beds are detailed in Figure 10. **F**) Close-up of area marked by rectangle in D, showing discs between thin layers of marl with silt grains (grey layers). **G**) Close-up of area marked by rectangle in F, showing the terminal edge of a discoidal structure. Note that overlying sedimentary laminae warp around the discoidal structure. **H**) Close-up of area marked by rectangle in G, showing that the discoidal structure is composed of a light-colored cement-dominated material, and the sediment above and below is dark-colored. The lens cap in (A) is 5 cm in diameter and the coin in (C) is 2 cm in diameter. Key: gml = gray mudstone layer; bol = black organic laminae.

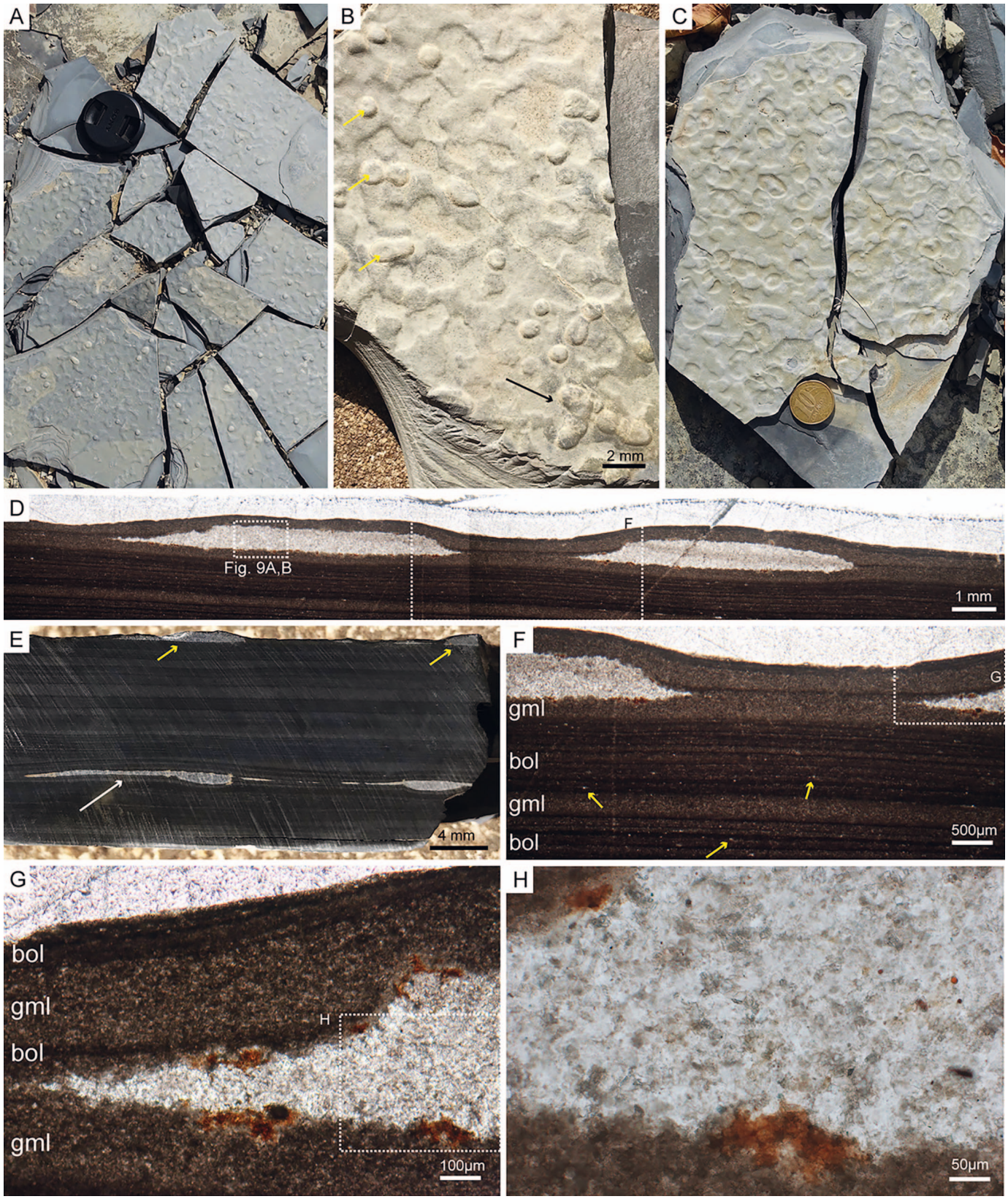

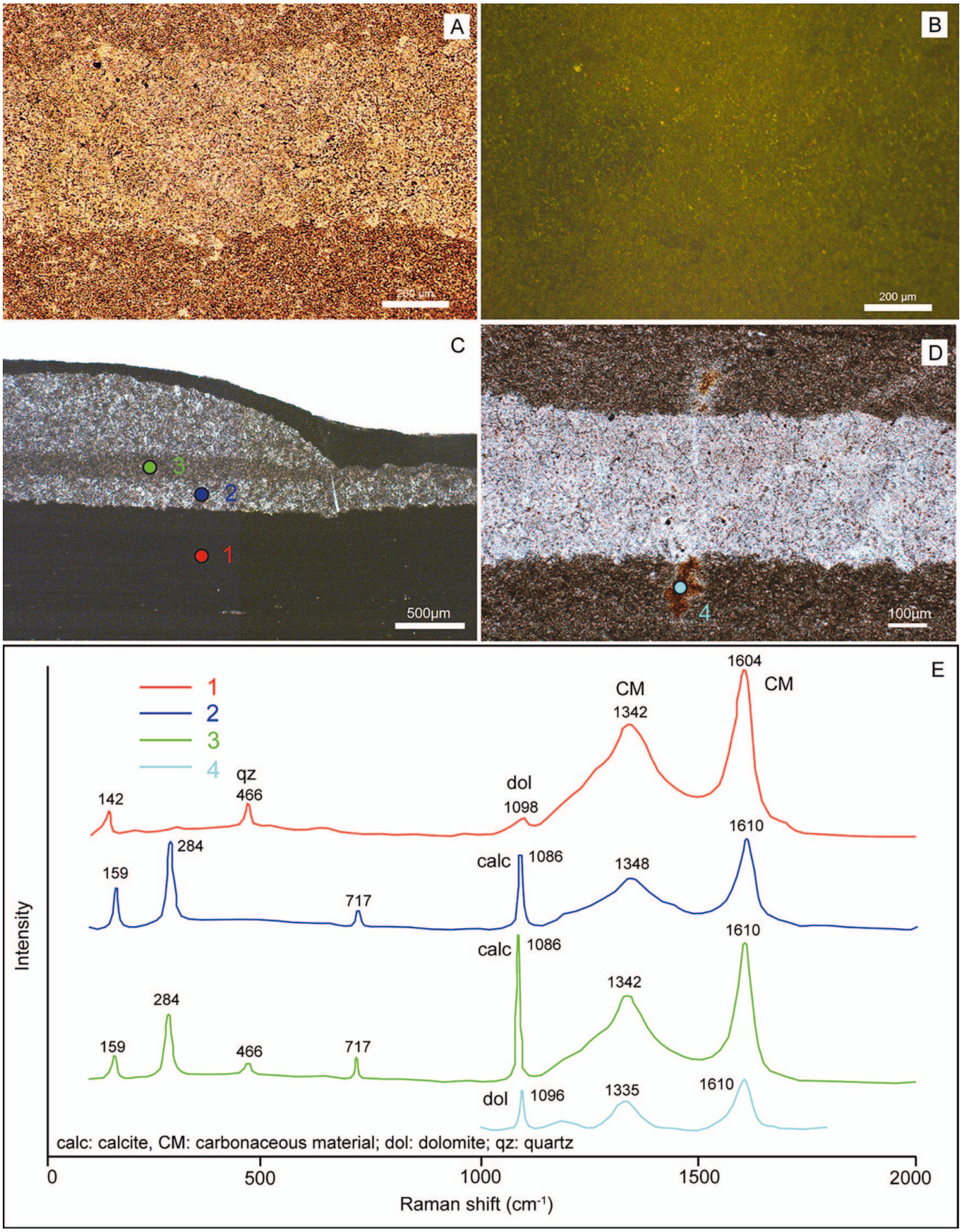

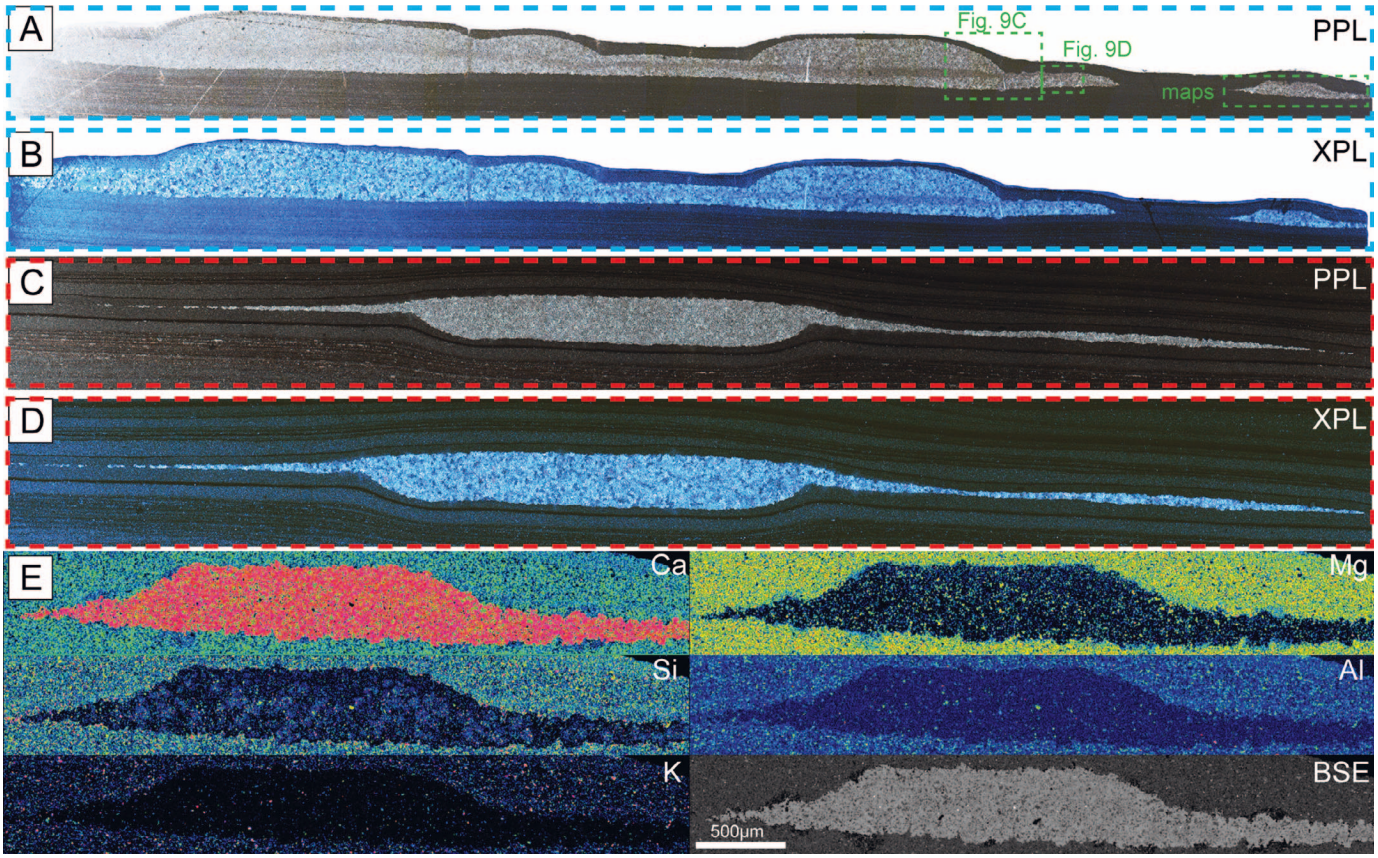


FIG. 10.—Parallel- (PPL) and cross-polarized (XPL) light microscopic images, back-scattered electron (BSE) microscopic image, and elemental maps of thin section prepared from slab illustrated in Figure 8E, showing the upper and lower beds bearing Type 2 discoidal structures from the Serra de Santa Helena Formation at the Pitarana section. **A**, **B**) Parallel- and cross-polarized light microscopic images of the upper disc-bearing bed. **C**, **D**) Parallel- and cross-polarized light microscopic images of the lower disc-bearing bed. **E**) Elemental maps and BSE image of the discoidal structure marked in A.

### *Discoidal Structures*

The four types of discoidal structures investigated in this study have similar size ranges, and can occur as negative hyporeliefs (Type 2) or positive epireliefs (Types 1, 2, 3, and 4). Despite their general discoidal geometry, these structures show a certain degree of morphological variation, sometimes showing an irregular or elongate morphology (e.g., Types 1 and 4). When densely distributed, these morphological variations seem to result from either mutual deformation or the partial merging of closely spaced structures (Figs. 6A, 8B, 10A, 10B).

Type 1 discs (Figs. 6, 7) are preserved exclusively in carbonate and marl facies. Although these discs are superficially similar in size, shape, and relief to Ediacaran macrofossils such as *Beltanelliformis* (Saint Martin and Saint Martin 2018), *Nemiana* (Ivantsov et al. 2014), and *Nimbia* (Néraudeau et al. 2018), they are more likely to be early diagenetic concretions resulting from differential cementation (Schwid et al. 2021). Unlike *Beltanelliformis* and *Nemiana*, Type 1 discoidal structures are preserved as positive epirelief features, and do not preserve concentric folds or wrinkles that could indicate the presence of an organic wall (Ivantsov et al. 2014). In vertical cross-sections, there are no discernable boundaries between these structures; instead, they form a continuous bed consisting of light-colored carbonate sediments and cements (Fig. 6B–6E). Finally, carbonate material from the discoidal structures and underlying sediment has similar $\delta^{13}C$ values (Fig. 6B), indicating a common source of alkalinity for carbonate precipitation. These observations indicate that, although Type 1 discoidal structures resemble early diagenetic concretions on bedding surface view, they do not form discrete structures in vertical cross-section views; thus, the disc-bearing layers were probably cemented during early diagenesis, prior to the cementation of underlying and overlying layers. The early diagenetic cementation was probably facilitated by microbial activities (e.g., microbial sulfate reduction), as suggested by the presence of oxidized pyrite framboids (Fig. 7C–7E).

Type 2 discoidal structures (Figs. 8–10) are filled with light-colored carbonate material (with calcite and organic matter) in sharp contrast with the dark-colored host rock (with dolomite, siliciclastic material, and organic matter) (Fig. 9E). The warping microlaminae above and below the discoidal structures (Fig. 8D, 8F) indicate that lithification of the discs predated sediment compaction. Terrigenous or carbonate mud may have

←

FIG. 9.—Type 2 discoidal structures from the Serra de Santa Helena Formation at the Pitarana section. **A**, **B**) Close-up views of area marked by rectangle in Figure 8D. Bright-field light microscopic image (A) and corresponding epifluorescence microscopic image (B) showing the contact between a discoidal structure and the host rock. **C**, **D**) Close-up views of areas marked by rectangles in Figure 10A; (C) cross-section showing the flat lower boundary of a disc and the sharp contact between the disc and the surrounding rock. Raman spectroscopic analyses were carried out on the marked spots; (D) parallel-polarized light microscopic image showing a fracture cutting the discoidal structure and filled with brownish material containing carbonaceous material (CM). **E**) Raman spectra corresponding to spots marked C and D. Note that carbonaceous material is present within the disc and in the matrix.

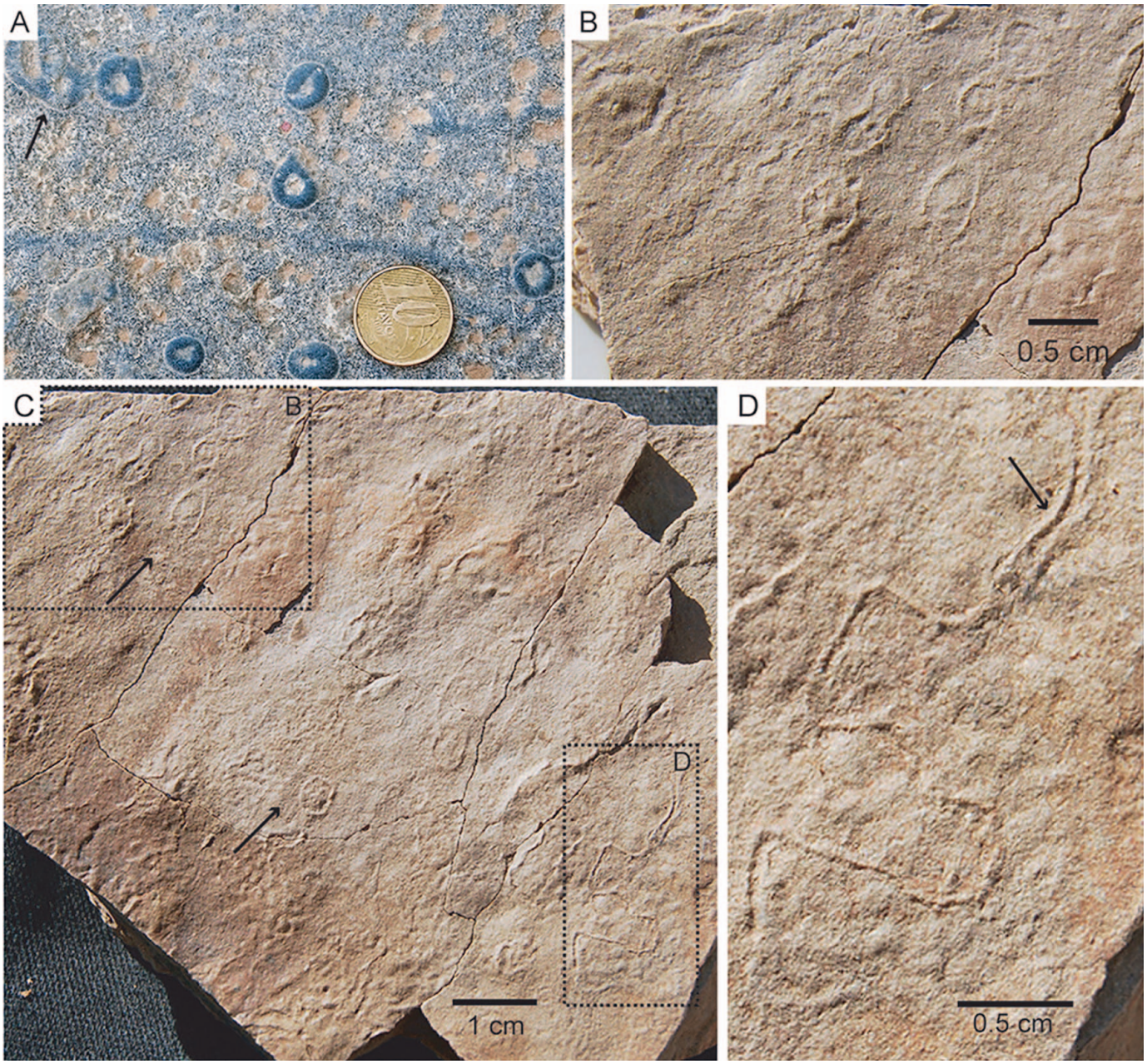


FIG. 11.—Discoidal structures and simple trails from the Serra de Santa Helena Formation at Lontra section. **A**) C- and donut-like discoidal structures (Type 3), showing an incomplete or a complete ring around a central depression. Note that discs occasionally deform each other or coalesce into more irregular structures (black arrow). Top bedding surface view. The coin is 2 cm in diameter. **B**) Close-up of C, showing *Nimbia*-like discoidal structures (Type 4) with a central flat area surrounded by a raised circular margin. The discs are preserved on the top bedding surface of fine sandstone and occur individually or in aggregates. **C**) Slightly rippled bedding surface containing wrinkles and discoidal structures (black arrows). Labeled rectangles mark areas shown in B and D. Top bedding surface view. **D**) Close-up of C, showing a possible trace fossil with slightly raised margins tentatively interpreted as lateral levees (black arrow).

acted as nuclei for cement precipitation, but they are not abundant. The interpretation is consistent with the abundance of calcite cement in discoidal structures (Fig. 10). The presence of patches of Fe oxides (interpreted as oxidized pyrite; Fig. 8G, 8H) near the boundary between the discoidal structures and the matrix is reminiscent of pyrite rims that may be present in some carbonate and chert concretions (Raiswell and Fisher 2000; Xiao et al. 2010). It is possible that lithification of the discoidal structures was driven by anaerobic oxidation of organic matter by sulfate reducing microbes during early diagenesis (Raiswell and Fisher 2000). Sulfate reduction coupled with pyrite precipitation can enhance pore-water alkalinity, thus promoting carbonate precipitation and the lithification of these discoidal structures (Canfield and Raiswell 1991; Visscher and Stolz 2005). Thus, we favor an abiotic origin for Type 2 discoidal structures (i.e., they do not represent holdfasts or other macroscopic organisms), although their formation may be related to the build-up of gases derived from organic matter degradation beneath a thin veneer of cohesive mat-sediment, and their preservation may have been facilitated by early lithification induced by microbial processes such as microbial sulfate reduction. Thus, this type of discoidal structures corresponds to biostabilization Type 2 of Noffke et al. (2022).

Type 3 discoidal structures (Fig. 11A) are characterized by a central depression, which may represent the collapsed conduit through which fluid escaped during sediment compaction (Dornbos et al. 2007; Callow et al. 2011; Menon et al. 2015, 2016; Inglez et al. 2022). Although this interpretation needs to be further tested with petrographic observation in thin sections, as has been done for Type 2 discs (Figs. 8–10), it is possible that fluids were trapped under well-developed biofilms or a thin cohesive layer covering the bedding surface, and they were forced to escape during sediment compaction.

Type 4 discoidal structures (Fig. 11B) are superficially similar to *Nimbia* (Néraudeau et al. 2018) in the presence of a flat central area surrounded by a thin circular rim. However, their morphology is more variable than *Nimbia*, since some specimens are elongate, irregular, and distributed on a chained-like pattern. Thus, these features are more likely to represent partially collapsed gas domes, developed by the accumulation of fluids derived from microbial metabolic processes beneath epibenthic mats. Given the delicate nature of these surficial textures and since the siliciclastic deposits are usually considered less prone to early cementation when compared with carbonate deposits, the flattened morphology of these discs may indicate poorer preservation of otherwise similarly developed features such as Types 2 and 3 discs.

### *Putative Trails or Sinusoidal Cracks?*

Shallow epirelief grooves with a curved to loosely meandering morphology (Fig. 11C, 11D) are somewhat similar to simple trails produced by epibenthic invertebrates (Jensen 2003; Buatois and Mángano 2011a; Gehling and Droser 2018). Their preservation on the top of sedimentary beds, as well as their raised margins, seemingly suggests active displacement of sedimentary material by a passing animal (Knox and Miller 1985; Jensen et al. 2005). Given the presence of putative lateral levees, a reasonable comparison can be made with ichnotaxa such as *Helminthopsis* isp. with a possible gradation to *Archaeonassa fossulata* at its terminal part.

On the other hand, the relatively abrupt turns (nearly 90°; Fig. 11D) are rather unusual for meandering trails produced by vermiform animals (Buatois and Mángano 2016), although a putative trace fossil described as *Vaqueroichnus stewarti* from the Neoproterozoic Mina el Mesquite Formation in Mexico (McMenamin 2016) also shows abrupt turns of approximate 90° to 120°. Because there is only a single available specimen that is morphologically simple, a critical assessment of alternative interpretations must be taken before further paleoecological and paleoenvironmental inferences are made. Sinusoidal cracks associated with cohesive sandy sediments due to the presence of EPS-rich microbial mats (Harazim et al. 2013; W.J. McMahon et al. 2017) can resemble the linear structure found in the Serra de Santa Helena Formation. These features, which can be preserved as curved grooves on top of sedimentary beds, are preferentially orientated parallel to the crests and troughs of rippled surface (Seilacher 2007). Indeed, similar sinusoidal cracks were originally reported as biogenic structures and often referred to as "*Manchuriophycus*" (Seilacher 2007; S. McMahon et al. 2017). Thus, it is possible that trail-like structure from the Serra de Santa Helena Formation may be considered broadly as microbially induced sedimentary structure. This interpretation is consistent with the co-occurrence of the trail-like structure with elephant skin-type surface texture that is generally considered as MISS. Another possibility is that the linear groove in the Serra de Santa Helena Formation may represent pseudotrails produced by rafting microbial fragments or aggregates in very shallow waters (Mariotti et al. 2016; Warren et al. 2020).

## FACIES DISTRIBUTION AND BIOGENICITY OF SURFACE SEDIMENTARY TEXTURES ON THE SERRA DE SANTA HELENA FORMATION

Mata and Bottjer (2013) proposed a facies model showing the environmental control for wrinkle structure formation and preservation, which can be applied here to illustrate the facies distribution of the microbial induced sedimentary structures in the Serra de Santa Helena Formation (Fig. 12). In their model, wrinkle structures are preferentially preserved in heterolithic beds deposited either in the offshore transition or tidal flat environments. In these settings, wrinkles are preserved at the interface between underlying sandstone and overlying siltstone or shale, similar to what we see in the Serra de Santa Helena Formation. This facies controlled distribution is hypothesized as a direct result of the preference of phototrophic microbes to colonize quartz-rich sandy substrates due to its high translucence (Noffke et al. 2002; Mata and Bottjer 2013). Also, the deposition of silt and/or mud under low energy conditions, covering microbially stabilized sand, further enhances the potential for microbial mat preservation (Mata and Bottjer 2009). Our observations are consistent with the Mata and Bottjer (2013) model and other studies (e.g., Mata and Bottjer 2009; Noffke et al. 2002) as the wrinkle structures and Type 4 discoidal structures of the Serra de Santa Helena Formation are also observed in heterolithic strata, probably associated to tidal flat environments. However, discoidal structures of the Types 1 to 3 associated to limestone and marl deposits are more likely associated with offshore transition environments.

Concerning the biogenicity of these structures, most of the surface textures described above can be classified as "Ba" (*sensu* Davies et al. 2016), as there is no unambiguous evidence to support either a definitive biotic or abiotic origin, although microbial activities likely played a direct or indirect role in their formation. The surface textures classified as Type 1 and 2 wrinkles are interpreted as related to disruption and plastic deformation analogous to small-scale cuspate or flame-like load casts developed under the influence of biostabilization by endobenthic mats. As such, these types of structures are the direct product of the interaction between biotic and physical processes within the depositional setting. On the other hand, Type 3 wrinkle structures are interpreted as surfaces colonized by epibenthic mats, and thus of essentially biologic origin ("B"). The distribution of these different types of sedimentary surface textures, and associated structures in vertical cross-section along distinct facies, can be considered to reflect variations in bathymetry and hydrodynamics within the inter- to supratidal zones (Noffke 2009, 2010).

The discoidal structures described in this paper may be interpreted as concretions (Type 1) or fluid escape structures (Types 2, 3, 4), although microbes may have played an indirect role through their metabolic production of gas and their extracellular polymeric substances. The comparison between Type 1 discs and Ediacaran body fossils is superficial and they unlikely share a similar origin, as the studied discoidal structures lack any concentric folds (which are a diagnostic feature of *Beltanelliformis* and *Nemiana*) and are preserved as positive epirelief features (as opposed to the typically positive hyporelief preservation mode of *Beltanelliformis* and *Nemiana*). Therefore, the discoidal structures from the Serra de Santa Helena Formation are classified as "A" or "Ab" *sensu* Davies et al. (2016).

The meandering groove structure is classified as "Ba" or "B". Possible interpretations include sinusoidal cracks analogous to "*Manchuriophycus*", or an affinity to the putative trace fossil *Vaqueiroichnus stewarti* or simple trails such as *Helminthopsis* and *Archaeonassa*.

Despite the uncertain origins of the structures described in this paper, most interpretations outlined above are either directly or indirectly related to microbial mats. Thus, it is safe to conclude that the Serra de Santa Helena Formation archives abundant sedimentary evidence for the extensive development of microbial mats in supra- to subtidal and offshore transition settings in the Ediacaran Bambuí basin.

## IMPLICATIONS FOR THE PALEOBIOLOGICAL RECORD OF THE BAMBUÍ BASIN

The upper Sete Lagoas Formation, the Serra de Santa Helena Formation, the Lagoa do Jacaré Formation, and the lower Serra da

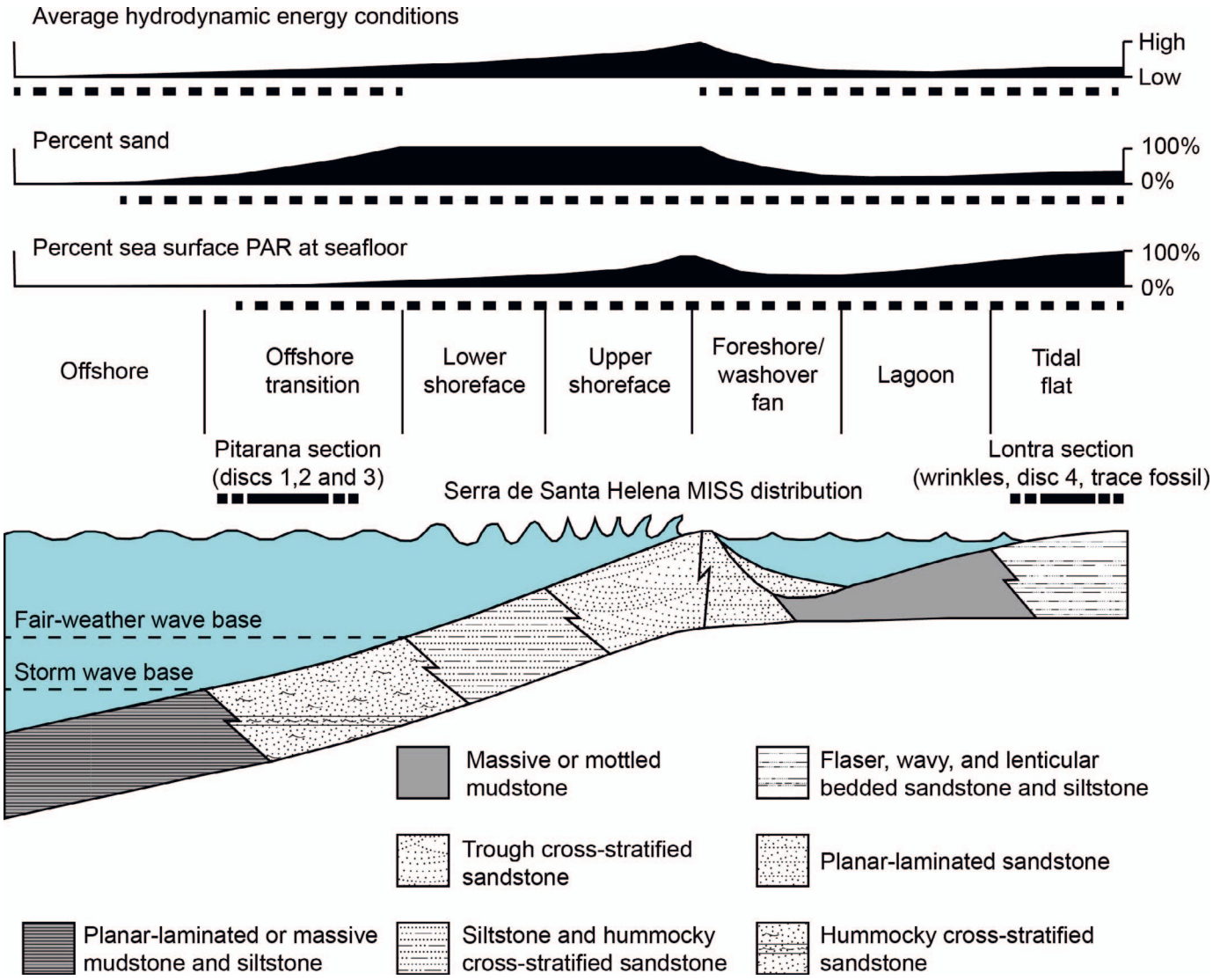


FIG. 12.—Facies model showing the distribution of MISS from the Serra de Santa Helena Formation. Modified from Mata and Bottjer (2013). Wrinkles and Type 4 discs from this study are found preferentially in heterolithic deposits in the tidal flat settings and Type 1–3 discs in the offshore transition. Key: PAR = photosynthetically active radiation.

Saudade Formation are characterized by anomalously high $\delta^{13}C_{carb}$ values. This anomaly is known as the Middle Bambuí Excursion or MIBE (Uhlein et al. 2019; Cui et al. 2020). In the Serra de Santa Helena Formation, the carbon isotopic values are consistently positive, varying between +7.3 to +12.5‰ (Uhlein et al. 2019), reflecting the climax of the MIBE. The anomalously high $\delta^{13}C_{carb}$ values have been interpreted as a result of deposition in a restricted and anoxic basin under the influence of water-column methanogenesis (Cui et al. 2020; Caetano-Filho et al. 2020). Based on geochemical data, Caetano-Filho et al. (2019, 2020) argued that hypersalinity, high alkalinity, anoxia, and active methanogenesis in a restricted basin may have led to stressful conditions that excluded eukaryotic life during the MIBE interval.

Abundant stromatolites are known from the Bambuí Group, particularly the Sete Lagoas, Lagoa do Jacaré, and upper Serra da Saudade formations (Vieira et al. 2007; Santos et al. 2018; Uhlein et al. 2020). However, eukaryotic fossils and particularly macroscopic animal fossils are rare in the Bambuí Group, either because of their poor preservation (Simonetti and Fairchild 2000; Warren et al. 2014), their rarity due to ecologically stressful environment (Caetano-Filho et al. 2019, 2020; Hippertt et al. 2019; Caxito et al. 2021), or inadequate sampling. On the other hand, the presence of microbially induced sedimentary structures in the Serra de Santa Helena Formation indicates extensive development of benthic microbial communities in shallow to moderately deep marine settings, similar to those described in modern environments with intense methanogenesis (Birgel et al. 2015). Microbial mats are thought to be conducive to the preservation of Ediacara-type macrofossils (Gehling 1999; Steiner and Reitner 2001; Droser et al. 2022). Thus, the profusion of MISS but the lack of macroscopic animal fossils in the Serra de Santa Helena Formation suggests that the environment was habitable to microbial communities but hostile to macroscopic animals.

The interactions between various microbial communities and different types of substrates led to the formation of a variety of microbially induced sedimentary surface textures described in this paper. The abundant MISS in the Serra de Santa Helena Formation are consistent with the interpretation of progressive restriction of the Bambuí basin (Paula-Santos et al. 2017; Caxito et al. 2021; Guacaneme et al. 2022), where typical late

Ediacaran and early Cambrian macrofaunas were not present, but benthic microbial assemblages thrived.

## CONCLUSIONS

The Serra de Santa Helena Formation of the Bambuí Group contains a wide range of structures formed through the interactions between microbial mats and physical processes. In this study, we integrate sedimentological observation, morphological description, and petrographic data to assess the distribution and origin of wrinkle, discoidal, and curvilinear groove structures from the Serra de Santa Helena Formation.

Wrinkle structures are found in both fine sandstone and siltstone deposits. Three morphotypes of wrinkle structures are described. Type 1 (honeycomb-like structures) and Type 2 (bulges and depressions) were only observed on sandstone beds. Type 3 (elephant skin-like structures) were only recovered from thin veneers of silt-grade sediment. These structures are interpreted as microbially induced sedimentary structures (MISS). In particular, the intricate patterns of Type 3 may represent fossilized epibenthic mats, developed in stable fine-grained supratidal settings. In contrast, Types 1 and 2 morphologies likely reflect biostabilization of sandy substrates by endobenthic microbial communities.

Four different types of discoidal structures were identified in fine sandstone, marl, and carbonate facies (Types 1–4). Despite morphological variations, Types 2, 3, and 4 may have a similar origin related to fluid accumulation in a sealed substrate underneath a cohesive microbial mat. Although Type 1 discoidal structures superficially resemble early diagenetic concretions, no well-defined boundaries were identified between discs. Instead, Type 1 discoidal structures form continuous beds dominated by calcite cements, indicating that selective cementation of the disc-bearing beds during early diagenesis may have played an important role. Regardless, microbial activities (e.g., microbial sulfate reduction) may have facilitated calcite precipitation and cementation, thus contributing to the formation of Type 1 discoidal structures. Thus, the formation of the discoidal structures is interpreted to be biotic-physical.

A meandering groove structure is reported from the Serra de Santa Helena Formation. It shares some similarities with simple trails such as *Helminthopsis* produced by epibenthic invertebrates; in particular, part of the groove is flanked by raised margins that are analogous to lateral levees and suggestive of sediment displacement by motile animals. The single available specimen and the unusual sharp turns, however, demands the consideration of alternative interpretations (e.g., grooves produced by rafting microbial aggregates or mat fragments).

The recognition of possible biotic structures in the Serra de Santa Helena Formation is important because they help to understand the benthic ecology of siliciclastic and carbonate substrates in the Bambuí basin at Ediacaran–Cambrian transition. Although the Serra de Santa Helena Formation may have been deposited in a restricted and anoxic basin that was hostile to macroscopic Ediacaran animals, microbial life thrived in the Bambuí basin.

## ACKNOWLEDGMENTS

This study was funded by São Paulo Research Foundation (FAPESP) (grants 2015/07391-0, 2017/19023-1, 2018/26230-6), CNPq (grant 444070/2014-1), and Petrobras (Sigitec 2014/-00519-9). The authors thank Dr. Anelize Bahniuk for the C and O isotope analyses performed at LAMIR (UFPR), Dr. Mitsuru Arai for the epifluorescence analysis, and the Center of Geosciences Applied to Petroleum Geology–UNESPetro for providing laboratory facilities. LVW is a research fellow of CNPq. GJU acknowledges the support of CNPq (432556/2018-4) and FAPEMIG (APQ-02240-21). SX was supported by the National Science Foundation (EAR-2021207). Editor Soren Jensen, reviewer Sean McMahon, and an anonymous reviewer are thanked for their constructive reviews that improved the manuscript. JO acknowledges the financial support provided by the PRH-ANP (National Agency of Petroleum, Natural Gas and Biofuels) and FINEP (Studies and Projects Funding) through her PRH-40 post-doctoral scholarship.

## REFERENCES

Alvarenga, C.J.S.S., Santos, R. V., Vieira, L.C., Lima, B.A.F.F., and Mancini, L.H., 2014, Meso-Neoproterozoic isotope stratigraphy on carbonates platforms in the Brasilia belt of Brazil: Precambrian Research, v. 251, p. 164–180, doi: 10.1016/j.precamres.2014.06.011.

Anderson, R.P., Tarhan, L.G., Cummings, K.E., Planavsky, N.J., and Bjornerud, M., 2016, Macroscopic structures in the 1.1 Ga continental Copper Harbor Formation: concretions or fossils?: PALAIOS, v. 31, p. 327–338.

Birgel, D., Meister, P., Lundberg, R., Horath, T.D., Bontognali, T.R.R., Bahniuk, A.M., de Rezende, C.E., Vasconcelos, C., and Mckenzie, J.A., 2015, Methanogenesis produces strong $^{13}C$ enrichment in stromatolites of Lagoa Salgada, Brazil: a modern analogue for Palaeo-/Neoproterozoic stromatolites? Geobiology, v. 13, p. 245–266, doi: 10.1111/gbi.12130.

Bobrovskiy, I., Hope, J.M., Krasnova, A., Ivantsov, A., and Brocks, J.J., 2018, Molecular fossils from organically preserved Ediacara biota reveal cyanobacterial origin for *Beltanelliformis*: Nature Ecology and Evolution, v. 2, p. 437–440.

Bosak, T., Bush, J.W.M., Flynn, M.R., Liang, B., Ono, S., Petroff, A.P., and Sim, M.S., 2010, Formation and stability of oxygen-rich bubbles that shape photosynthetic mats: Geobiology, v. 8, p. 45–55, doi: 10.1111/j.1472-4669.2009.00227.x.

Bouougri, E. and Porada, H., 2002, Mat-related sedimentary structures in Neoproterozoic peritidal passive margin deposits of the West African Craton (Anti-Atlas, Morocco): Sedimentary Geology, v. 153, p. 85–106.

Bouougri, E.H. and Porada, H., 2007, Siliciclastic biolaminites indicative of widespread microbial mats in the Neoproterozoic Nama Group of Namibia: Journal of African Earth Sciences, v. 48, p. 38–48, doi: 10.1016/j.jafrearsci.2007.03.004.

Buatois, L.A. and Mángano, M.G., 2011a, Ichnology: Organism-Substrate Interactions in Space and Time: Cambridge University Press, Cambridge, 358 p.

Buatois, L.A. and Mángano, M.G., 2011b, The trace-fossil record of organism-matground interactions in space and time, *in* N. Noffke and H. Chafetz (eds.), Microbial Mats in Siliciclastic Depositional Systems through Time: SEPM Special Publication 101, p. 15–28.

Buatois, L.A. and Mángano, M.G., 2016, Ediacaran ecosystems and the dawn of animals, *in* M.G. Mángano and L.A. Buatois (eds.), The Trace-Fossil Record of Major Evolutionary Events: Springer, Dordrecht, p. 27–72.

Buatois, L.A., Narbonne, G.M., Mángano, M.G., Carmona, N.B., and Myrow, P., 2014, Ediacaran matground ecology persisted into the earliest Cambrian: Nature Communications, v. 5, p. 3544, doi: 10.1038/ncomms4544.

Bykova, N., Gill, B.C., Grazhdankin, D., Rogov, V., and Xiao, S., 2017, A geochemical study of the Ediacaran discoidal fossil *Aspidella* preserved in limestones: implications for its taphonomy and paleoecology: Geobiology, v. 15, p. 572–587.

Caetano-Filho, S., Paula-Santos, G.M., Guacaneme, C., Babinski, M., Bedoya-Rueda, C., Peloso, M., Amorim, K., Afonso, J., Kuchenbecker, M., Reis, H., and Trindade, R.I.F., 2019, Sequence stratigraphy and chemostratigraphy of an Ediacaran–Cambrian foreland-related carbonate ramp (Bambuí Group, Brazil): Precambrian Research, v. 331, article 105365, doi: 10.1016/j.precamres.2019.105365.

Caetano-Filho, S., Sansjofre, P., Ader, M., Paula-Santos, G., Babinski, M., Bedoya-Rueda, C., and Kuchenbecker, M., 2020, A large epeiric methanogenic Bambuí sea in the core of Gondwana supercontinent?: Geoscience Frontiers, v. 12, p. 203–218, doi: 10.1016/j.gsf.2020.04.005.

Callow, R.H.T., Battison, L., and Brasier, M.D., 2011, Diverse microbially induced sedimentary structures from 1Ga lakes of the Diabaig Formation, Torridon Group, northwest Scotland: Sedimentary Geology, v. 239, p. 117–128, doi: 10.1016/j.sedgeo.2011.06.002.

Canfield, D.E. and Raiswell, R., 1991, Carbonate precipitation and dissolution, its relevance to fossil preservation, *in* P.A. Allison and D.E.G. Briggs (eds.), Taphonomy: Releasing the Data Locked in the Fossil Record: Topics in Geobiology, v. 9, Plenum Press, New York p. 411–453.

Caxito, F.A., Frei, R., Uhlein, G.J., Gonçalves Dias, T., Árting, T.B., Uhlein, A., Dias, T.G., Árting, T.B., and Uhlein, A., 2018, Multiproxy geochemical and isotope stratigraphy records of a Neoproterozoic oxygenation event in the Ediacaran Sete Lagoas cap carbonate, Bambuí Group, Brazil: Chemical Geology, v. 481, p. 119–132, doi: 10.1016/j.chemgeo.2018.02.007.

Caxito, F. Halverson, de A., Uhlein, G.P., Stevenson, A., Gonçalves R., Dias, T., and Uhlein, G.J., 2012, Marinoan glaciation in east central Brazil: Precambrian Research, v. 200–203, p. 38–58, doi: 10.1016/j.precamres.2012.01.005.

Caxito, F., Lana, C., Frei, R., Uhlein, G.J., Sial, A.N., Dantas, E.L., Pinto, A.G., Campos, F.C., Galvão, P., Warren, L. V., Okubo, J., and Ganade, C.E., 2021, Goldilocks at the dawn of complex life: mountains might have damaged Ediacaran–Cambrian ecosystems and prompted an early Cambrian greenhouse world: Scientific Reports, v. 11, p. 1–15, doi: 10.1038/s41598-021-99526-z.

Crockford, P.W., Hodgskiss, M.S.W., Uhlein, G.J., Caxito, F., Hayles, J.A., and Halverson, G.P., 2018, Linking paleocontinents through triple oxygen isotope anomalies: Geology, v. 46, p. 8–11.

Cuadrado, D.G., Perillo, G.M.E., and Vitale, A.J., 2014, Modern microbial mats in siliciclastic tidal flats: evolution, structure and the role of hydrodynamics: Marine Geology, v. 352, p. 367–380, doi: 10.1016/j.margeo.2013.10.002.

Cui, H., Warren, L.V., Uhlein, G.J., Okubo, J., Liu, X.M., Plummer, R.E., Baele, J.M., Goderis, S., Claeys, P., and Li, F., 2020, Global or regional? Constraining the origins of the middle Bambuí carbon cycle anomaly in Brazil: Precambrian Research, v. 348, article 105861, doi: 10.1016/j.precamres.2020.105861.

Dardenne, M.A., 1978, Síntese sobre a estratigrafia do Grupo Bambuí no Brasil Central, *in* Congresso Brasileiro de Geologia: 30° Anais, Recife, Brazil, p. 597–610.

Dardenne, M.A. and Campos Neto, M.C., 1975, Estromatólitos colunares na série Minas (MG): Revista Brasileira de Geociências, v. 5, p. 99–105.

Davies, N.S., Liu, A.G., Gibling, M.R., and Miller, R.F., 2016, Resolving MISS conceptions and misconceptions: a geological approach to sedimentary surface textures generated by microbial and abiotic processes: Earth-Science Reviews, v. 154, p. 210–246.

Dornbos, S.Q., Noffke, N., and Hagadorn, J.W., 2007, Mat-decay features, *in* J. Schieber, P.K. Bose, P.G. Eriksson, S. Banjeree, S. Sarkar, W. Altermann, and O. Catuneanu (eds.), Atlas of Microbial Mat Features Preserved within the Clastic Rock Record: Elsevier, Amsterdam, p. 106–110.

Droser, M.L., Evans, S.D., Tarhan, L.G., Surprenant, R.L., Hughes, I. V., Hughes, E.B., and Gehling, J.G., 2022, What happens between depositional events, stays between depositional events: the significance of organic mat surfaces in the capture of Ediacara communities and the sedimentary rocks that preserve them: Frontiers in Earth Science, v. 10, p. 1–17, doi: 10.3389/feart.2022.826353.

Fairchild, T.R. and Sanchez, E.A.., 2015, Microbialitos no Brasil: panorâmica de ocorrências e guia de caracterização morfológica, *in* T.R. Fairchild, R. Rohn, and D. Dias-Brito (eds.), Microbialitos Do Brasil: Do Pré-Cambriano Ao Recente: IGCE/UNESP Rio Claro, p. 22–41.

Fairchild, T.R., Schopf, J.W., Shen-Miller, J., Guimarães, E.M., Edwards, M.D., Lagstein, A., Xiao, L., Pabst, M., and Melo-Filho, L.S., 1996, Recent discoveries of Proterozoic microfossils in south-central Brazil: Precambrian Research, v. 80, p. 125–152, doi: 10.1016/S0301-9268(96)00009-5.

Fairchild, T.R. and Subacius, S.M.R., 1986, Microfossils associated with silicified *Stratifera undata* Komar 1966 from the late Proterozoic Bambuí Group, south-central Brazil: Precambrian Research, v. 33, p. 323–339.

Fragoso, D.G.C., Uhlein, A., Sanglard, J.C.D., Suckau, G.L., Guerzoni, H.T.G., and Faria, P.H., 2011, Geologia dos Grupos Bambuí, Areado e Mata da Corda na Folha Presidente Olegário (1:100.000), Mg: Registro deposicional do Neoproterozóico ao Neocretáceo da Bacia do São Francisco: Geonomos, v. 19, p. 28–38, doi: 10.18285/geonomos.v19i1.60.

Gehling, J.G., 1999, Microbial mats in terminal Proterozoic siliciclastics: Ediacaran death masks: PALAIOS, v. 14, p. 40–57, doi: 10.2307/3515360.

Gehling, J.G. and Droser, M.L., 2009, Textured organic surfaces associated with the Ediacara biota in South Australia: Earth-Science Reviews, v. 96, p. 196–206.

Gehling, J.G. and Droser, M.L., 2018, Ediacaran scavenging as a prelude to predation: Emerging Topics in Life Sciences, v. 2, p. 213–222, doi: 10.1042/ETLS20170166.

Gehling, J.G., Narbonne, G.M., and Anderson, M.M., 2000, The first named Ediacaran body fossil, *Aspidella terranovica*: Palaeontology, v. 43, p. 427–456, doi: 10.1111/j.0031-0239.2000.00134.x.

Gerdes, G., Klenke, T., and Noffke, N., 2000, Microbial signatures in peritidal siliciclastic sediments: a catalogue: Sedimentology, v. 47, p. 279–308.

Gingras, M., Hagadorn, J.W., Seilacher, A., Lalonde, S.V., Pecoits, E., Petrash, D., and Konhauser, K.O., 2011, Possible evolution of mobile animals in association with microbial mats: Nature Geoscience, v. 4, p. 372–375, doi: 10.1038/ngeo1142.

Grazhdankin, D. and Gerdes, G., 2007, Ediacaran microbial colonies: Lethaia, v. 40, p. 201–210, doi: 10.1111/j.1502-3931.2007.00025.x.

Guacaneme, C., Babinski, M., Bedoya-Rueda, C., Paula-Santos, G.M., Caetano-Filho, S., Kuchenbecker, M., Reis, H.L.S., and Trindade, R.I.F., 2021, Tectonically-induced strontium isotope changes in ancient restricted seas: ghe case of the Ediacaran–Cambrian Bambuí foreland basin system, east Brazil: Gondwana Research, v. 93, p. 275–290.

Guacaneme, C., Caetano-Filho, S., Paula-Santos, G.M., Babinski, M., Fraga-Ferreira, P.L., Bedoya-Rueda, C., Kuchenbecker, M., Reis, H.L.S., and Trindade, R.I.F., 2022, Paleoenvironmental redox evolution of Ediacaran–Cambrian restricted seas in the core of West Gondwana: insights from trace-metal geochemistry and stratigraphy of the Bambuí Group, east Brazil: Journal of South American Earth Sciences, v. 119, article 103998, doi: 10.1016/j.jsames.2022.103998.

Hagadorn, J.W. and Bottjer, D.J., 1997, Wrinkle structures: microbially mediated sedimentary structures common in subtidal siliciclastic settings at the Proterozoic–Phanerozoic transition: Geology, v. 25, p. 1047–1050.

Hagadorn, J.W. and Bottjer, D.J., 1999, Restriction of a Late Neoproterozoic Biotope: suspect-microbial structures and trace fossils at the Vendian-Cambrian transition: PALAIOS, v. 14, p. 73.

Hagadorn, J.W. and Miller, R.F., 2011, Hypothesized Cambrian Medusae from Saint John, New Brunswick, reinterpreted as sedimentary structures: Atlantic Geology, v. 47, p. 66–80, doi: 10.4138/atlgeol.2011.002.

Harazim, D., Callow, R.H.T.T., and Mcilroy, D., 2013, Microbial mats implicated in the generation of intrastratal shrinkage ('synaeresis') cracks: Sedimentology, v. 60, p. 1621–1638, doi: 10.1111/sed.12044.

Hippertt, J.P., Caxito, F.A., Uhlein, G.J., Nalini, H.A., Sial, A.N., Abreu, A.T., and Nogueira, L.B., 2019, The fate of a Neoproterozoic intracratonic marine basin: trace elements, TOC and iron speciation geochemistry of the Bambuí Basin, Brazil: Precambrian Research, v. 330, p. 101–120, doi: 10.1016/j.precamres.2019.05.001.

Iglesias, M. and Uhlein, A., 2009, Estratigrafia do Grupo Bambuí e coberturas fanerozóicas no vale do rio São Francisco, norte de Minas Gerais: Revista Brasileira de Geociências, v. 39, p. 256–266.

Inglez, L., Warren, L.V., Okubo, J., Simões, M.G., Quaglio, F., Arrouy, M.J., and Netto, R.G., 2019, Discs and discord: the paleontological record of Ediacaran discoidal structures in the south American continent: Journal of South American Earth Sciences, v. 89, p. 319–336, doi: 10.1016/j.jsames.2018.11.023.

Inglez, L., Warren, L. V., Quaglio, F., Netto, R.G., Okubo, J., Arrouy, M.J., Simões, M.G., and Poiré, D.G., 2022, Scratching the discs: evaluating alternative hypotheses for the origin of the Ediacaran discoidal structures from the Cerro Negro Formation, la Providencia Group, Argentina: Geological Magazine, v. 159, p. 1192–1209. doi: 10.1017/S0016756821000327.

Ivantsov, A.Y., Gritsenko, V.P., Konstantinenko, L.I., and Zakrevskaya, M.A., 2014, Revision of the problematic Vendian macrofossil *Beltanelliformis* (=*Beltanelloides*, Nemiana): Paleontological Journal, v. 48, p. 1415–1440, doi: 10.1134/S0031030114130036.

Jensen, S., 2003, The Proterozoic and earliest Cambrian trace fossil record: patterns, problems and perspectives: Integrative and Comparative Biology, v. 43, p. 219–228, doi: 10.1093/icb/43.1.219.

Jensen, S., Droser, M.L., and Gehling, J.G., 2005, Trace fossil preservation and the early evolution of animals: Palaeogeography, Palaeoclimatology, Palaeoecology, v. 220, p. 19–29, doi: 10.1016/j.palaeo.2003.09.035.

Knoll, A.H., Wörndle, S., and Kah, L.C., 2013, Covariance of microfossil assemblages and microbialite textures across an upper mesoproterozoic carbonate platform: PALAIOS, v. 28, p. 453–470, doi: 10.2110/palo.2013.p13-005r.

Knox, L.W. and Miller, M.F., 1985, Environmental control of trace fossil morphology, *in* H.A. Curran (ed.), Biogenic Structures: Their Use in Interpreting Depositional Environments: SEPM Special Publication 35, p. 167–176.

Kolesnikov, A.V., Danelian, T., Gommeaux, M., Maslov, A.V., and Grazhdankin, D.V., 2017, Arumberiamorph structure in modern microbial mats: implications for Ediacaran paleobiology: Bulletin de la Societe Geologique de France, v. 188, p. 1–10, doi: 10.1051/bsgf/2017006.

Kolesnikov, A. V, Grazhdankin, D. V, and Maslov, A. V, 2012, Arumberia-type structures in the Upper Vendian of the Urals: Doklady Earth Sciences, v. 447, p. 1233–1239.

Kuchenbecker, M., Babinski, M., Pedrosa-Soares, A.C., Lopes-Silva, L., and Pimenta, F., 2016, Chemostratigraphy of the lower Bambuí Group, southwestern São Francisco Craton, Brazil: insights on Gondwana paleoenvironments: Brazilian Journal of Geology, v. 46, p. 145–162, doi: 10.1590/2317-488920160030285.

Kumar, S. and Ahmad, S., 2014, Microbially induced sedimentary structures (MISS) from the Ediacaran Jodhpur Sandstone, Marwar Supergroup, western Rajasthan: Journal of Asian Earth Sciences, v. 91, p. 352–361.

Luo, C., Zhu, M., and Reitner, J., 2016, The Jinxian Biota revisited: taphonomy and body plan of the Neoproterozoic discoid fossils from the southern Liaodong Peninsula, North China: Palaontologische Zeitschrift, v. 90, p. 205–224.

Mángano, M.G. and Buatois, L.A., 2016, The Cambrian explosion, *in* M.G. Mángano and L.A. Buatois (eds.), The Trace-Fossil Record of Major Evolutionary Events: Topics on Geobiology, v. 39, Springer, p. 73–126.

Mariotti, G., Pruss, S.B., Ai, X., Perron, J.T., and Bosak, A.T., 2016, Microbial origin of early animal trace fossils?: Journal of Sedimentary Research, v. 86, p. 287–293, doi: 10.2110/jsr.2016.19.

Mata, S.A. and Bottjer, D.J., 2009, The paleoenvironmental distribution of Phanerozoic wrinkle structures: Earth-Science Reviews, v. 96, p. 181–195, doi: 10.1016/j.earscirev.2009.06.001.

Mata, S.A. and Bottjer, D.J., 2013, Facies control on lower Cambrian wrinkle structure development and paleoenvironmental distribution, southern Great Basin, United States: Facies, v. 59, p. 631–651, doi: 10.1007/s10347-012-0331-3.

Mata, S.A., Harwood, C.L., Corsetti, F.A., Stork, N.J., Eilers, K., Berelson, W.M., and Spear, J.R., 2012, Influence of gas production and filament orientation on stromatolite microfabric: PALAIOS, v. 27, p. 206–219, doi: 10.2110/palo.2011.p11-088r.

McIlroy, D., Crimes, T.P., and Pauley, J.C., 2005, Fossils and matgrounds from the Neoproterozoic Longmyndian Supergroup, Shropshire, UK: Geological Magazine, v. 142, p. 441–455.

McMahon, W.J., Davies, N.S., and Went, D.J., 2017, Negligible microbial matground influence on pre-vegetation river functioning: evidence from the Ediacaran–Lower Cambrian Series Rouge, France: Precambrian Research, v. 292, p. 13–34, doi: 10.1016/j.precamres.2017.01.020.

McMahon, S., Hood, A.V.S., and McIlroy, D., 2017, The origin and occurrence of subaqueous sedimentary cracks: Geological Society, London, Special Publications, v. 448, p. 285–309, doi: 10.1144/SP448.15.

McMenamin, M.A.S., 2016, Mat farmers, *in* Dynamic Paleontology: Springer International Publishing, Switzerland, p. 79–96, doi: 10.1007/978-3-319-22777-1_1.

Menon, L.R., McIlroy, D., and Brasier, M.D., 2016, "Intrites" from the Ediacaran Longmyndian Supergroup, UK: a new form of microbially-induced sedimentary structure (MISS): Geological Society Special Publication, v. 448, p. 271–283.

Menon, L.R., McIlroy, D., Liu, A.G., and Brasier, M.D., 2015, The dynamic influence of microbial mats on sediments: fluid escape and pseudofossil formation in the Ediacaran Longmyndian Supergroup, UK: Journal of the Geological Society, v. 173, p. 177–185.

Meyer, M., Xiao, S., Gill, B.C., Schiffbauer, J.D., Chen, Z., Zhou, C., and Yuan, X., 2014, Interactions between Ediacaran animals and microbial mats: insights from *Lamonte trevallis*, a new trace fossil from the Dengying Formation of South China: Palaeogeography, Palaeoclimatology, Palaeoecology, v. 396, p. 62–74, doi: 10.1016/j.palaeo.2013.12.026.

Moreira, D.S., Uhlein, A., Dussin, I.A., Uhlein, G.J., and Misuzaki, A.M.P., 2020, A Cambrian age for the upper Bambuí Group, Brazil, supported by the first U-Pb dating of volcanoclastic bed: Journal of South American Earth Sciences, article 102503, doi: 10.1016/j.jsames.2020.102503.

Néraudeau, D., Dabard, M.P., El Albani, A., Gougeon, R., Mazurier, A., Pierson-Wickmann, A.C., Poujol, M., Saint Martin, and Saint Martin, J.P.,S., 2018, First evidence of Ediacaran–Fortunian elliptical body fossils in the Brioverian series of Brittany, NW France: Lethaia, v. 51, p. 513–522, doi: 10.1111/let.12270.

Noffke, N., 1998, Multidirected ripple marks rising from biological and sedimentological processes in modern lower supratidal deposits (Mellum Island, southern North Sea): Geology, v. 26, p. 879–882, doi: 10.1130/0091-7613(1998)026<0879:MRMRFB>2.3.CO;2.

Noffke, N., 1999, Erosional remnants and pockets evolving from biotic-physical interactions in a recent lower supratidal environment: Sedimentary Geology, v. 123, p. 175–181, doi: 10.1016/S0037-0738(98)00135-3.

Noffke, N., 2009, The criteria for the biogeneicity of microbially induced sedimentary structures (MISS) in Archean and younger, sandy deposits: Earth-Science Reviews, v. 96, p. 173–180, doi: 10.1016/j.earscirev.2008.08.002.

Noffke, N., 2010, Geobiology: Microbial mats in sandy deposits from the Archean Era to today: Springer, Heidelberg, 194 p.

Noffke, N., 2018, Comment on the paper by Davies et al. "Resolving MISS conceptions and misconceptions: A geological approach to sedimentary surface textures generated by microbial and abiotic processes" (Earth Science Reviews, 154 (2016), 210–246): Earth-Science Reviews, v. 176, p. 373–383, doi: 10.1016/j.earscirev.2017.11.021.

Noffke, N., 2021, Microbially induced sedimentary structures in clastic deposits: implication for the prospection for fossil life on Mars: Astrobiology, v. 21, p. 866–892, doi: 10.1089/ast.2021.0011.

Noffke, N., Beraldi-Campesi, H., Callefo, F., Carmona, N., Cuadrado, D.G., Hickman-Lewis, K., Homann, M., Mitchell, R., Sheldon, N., Westall, F., and Xiao, S., 2022, Part B, Volume 2, Chapter 5: Microbially induced sedimentary structures (MISS): Treatise Online, p. 1–29, http://rid.unrn.edu.ar/handle/20.500.12049/9065.

Noffke, N., Gerdes, G., Klenke, T., and Krumbein, W.E., 1996, Microbially induced sedimentary structures—examples from modern sediments of siliciclastic tidal flats: Zentralblatt für Geologie und Palaeontologie Teil I, v. 1, p. 307–316.

Noffke, N., Knoll, A.H., and Grotzinger, J.P., 2002, Sedimentary controls on the formation and preservation of microbial mats in siliciclastic deposits: a case study from the Upper Neoproterozoic Nama Group, Namibia: PALAIOS, v. 17, p. 533–544, doi: 10.1669/0883-1351(2002)017<0533:SCOTFA>2.0.CO;2.

Nogueira, A.C.R., Riccomini, C., Nóbrega Sial, A., Veloso Moura, C.A., and Fairchild, T.R., 2003, Soft-sediment deformation at the base of the Neoproterozoic Puga cap carbonate (southwestern Amazon craton, Brazil): confirmation of rapid icehouse to greenhouse transition in Snowball Earth: Geology, v. 31, p. 613–616, doi: 10.1130/0091-7613(2003)031<0613:SDATBO>2.0.CO;2.

O'Neil, G.R., Tackett, L.S., and Meyer, M., 2020, Petrographic evidence for Ediacaran microbial mat-targeted behaviors from the Great Basin, United States: Precambrian Research, v. 345, article 105768, doi: 10.1016/j.precamres.2020.105768.

Okubo, J., Muscente, A.D., Luvizotto, G.L., Uhlein, G.J., and Warren, L.V., 2018, Phosphogenesis, aragonite fan formation and seafloor environments following the Marinoan glaciation: Precambrian Research, v. 311, p. 24–36, doi: 10.1016/j.precamres.2018.04.002.

Okubo, J., Warren, L.V., Luvizotto, G.L., Varejão, F.G., Quaglio, F., Uhlein, G.J., and Assine, M.L., 2020, Evidences of seismic events during the sedimentation of Sete Lagoas Formation (Bambuí Group–Ediacaran , Brazil) : Journal of South American Earth Sciences, v. 98, article 102461, doi: 10.1016/j.sames.2019.102461.

Paula-Santos, G.M., Babinski, M., Kuchenbecker, M., Caetano-Filho, S., Trindade, R.I., and Pedrosa-Soares, A.C., 2015, New evidence of an Ediacaran age for the Bambuí Group in southern São Francisco craton (eastern Brazil) from zircon U-Pb data and isotope chemostratigraphy: Gondwana Research, v. 28, p. 702–720, doi: 10.1016/j.gr.2014.07.012.

Paula-Santos, G.M., Caetano-Filho, S., Babinski, M., Trindade, R.I.F., and Guacaneme, C., 2017, Tracking connection and restriction of West Gondwana São Francisco Basin through isotope chemostratigraphy: Gondwana Research, v. 42, p. 280–305, doi: 10.1016/j.gr.2016.10.012.

Pemberton, S.G., Frey, R.W., and Bromley, R.G., 1988, The ichnotaxonomy of *Conostichus* and other plug-shaped ichnofossils: Canadian Journal of Earth Sciences, v. 25, p. 866–892, doi: 10.1139/e88-085.

Perrella, P., Uhlein, A., Uhlein, G.J., Sial, A.N., Pedrosa-Soares, A.C., and Lima, O.N.B., 2017, Facies analysis, sequence stratigraphy and chemostratigraphy of the Sete Lagoas Formation (Bambuí Group), northern Minas Gerais State, Brazil: evidence of a cap carbonate deposited on the Januária basement high: Brazilian Journal of Geology, v. 47, p. 59–77, doi: 10.1590/2317-4889201720160112.

Pflüger, F. and Gresse, P., 1996, Microbial sand chips—a non-actualistic sedimentary structure: Sedimentary Geology, v. 102, p. 263–274.

Porada, H. and Bouougri, E.H., 2007, Wrinkle structures-a critical review: Earth-Science Reviews, v. 81, p. 199–215, doi: 10.1016/j.earscirev.2006.12.001.

Porada, H. and Bouougri, E., 2008, Neoproterozoic trace fossils vs. microbial mat structures: examples from the Tandilia Belt of Argentina: Gondwana Research, v. 13, p. 480–487.

Porada, H., Ghergut, J., and Bouougri, E.H., 2008, Kinneyia-type wrinkle structures—critical review and model of formation: PALAIOS, v. 23, p. 65–77, doi: 10.2110/palo.2006.p06-095r.

Raiswell, R. and Fisher, Q.J., 2000, Mudrock-hosted carbonate concretions: a review of growth mechanisms and their influence on chemical and isotopic composition: Journal of the Geological Society, v. 157, p. 239–251, doi: 10.1144/jgs.157.1.239.

Romero, G.R., Sanchez, E.A.M., Morais, L., Boggiani, P.C., and Fairchild, T.R., 2016, Tubestone microbialite association in the Ediacaran cap carbonates in the southern Paraguay Fold Belt (SW Brazil): geobiological and stratigraphic implications for a Marinoan cap carbonate: Journal of South American Earth Sciences, v. 71, p. 172–181, doi: 10.1016/j.jsames.2016.06.014.

Saint Martin, and Saint Martin, J.P.S., 2018, *Beltanelliformis brunsae* Menner in Keller, Menner, Stepanov and Chumakov, 1974: an Ediacaran fossil from Neoproterozoic of Dobrogea (Romania): Geodiversitas, v. 40, p. 537–548.

Sallun Filho, W. and Fairchild, T., 2000, Stromatolites in the Mesoproterozoic Itaiacoca Group (SE Brazil): paleoenvironmental inferences and comparisons with other similar forms: Anais da Academia Brasileira de Ciências, v. 72, p. 602–603.

Sanchez, E.A.M., Uhlein, A., and Fairchild, T.R., 2021, *Treptichnus pedum* in the Três Marias Formation, south-central Brazil, and its implications for the Ediacaran–Cambrian transition in South America: Journal of South American Earth Sciences, v. 105, article 102983, doi: 10.1016/j.jsames.2020.102983.

Sanchez, E.A.M., Vieira, T.A., Reis, H.L.S., and Kuchenbecker, M., 2018, Microbialitos fósseis da Formação Jaíba, Grupo Bambuí, Minas Gerais, Brasil: Revista Brasileira de Paleontologia, v. 21, p. 175–186, doi: 10.4072/rbp.2018.2.07.

Santos, D.M., Sanchez, E.A.M., and Santucci, R.M., 2018, Morphological and petrographic analysis of newly identified stromatolitic occurrences in the Lagoa do Jacaré Formation, Bambuí Group, state of Minas Gerais, Brazil: Revista Brasileira de Paleontologia, v. 21, p. 195–207.

Santos, R.V., Souza de Alvarenga, C.J., Babinski, M., Ramos, M.L.S., Cukrov, N., Fonseca, M.A., da Nóbrega Sial, A., Dardenne, M.A., and Noce, C.M., 2004, Carbon isotopes of Mesoproterozoic–Neoproterozoic sequences from Southern São Francisco craton and Araçuaí Belt, Brazil: paleographic implications: Journal of South American Earth Sciences, v. 18, p. 27–39.

Schwid, M.F., Xiao, S., Nolan, M.R., An, Z., and Tech, V., 2021, Differential weathering of diagenetic concretions and the formation of Neoproterozoic annulated discoidal structures: PALAIOS, v. 36, p. 15–27.

Seilacher, A., 2007, Trace fossil Analysis: Springer Science and Business Media, Berlin, 238p.

Shepard, R.N. and Sumner, D.Y., 2010, Undirected motility of filamentous cyanobacteria produces reticulate mats: Geobiology, v. 8, p. 179–190, doi: 10.1111/j.1472-4669.2010.00235.x.

Simonetti, C. and Fairchild, T.R., 2000, Proterozoic microfossils from subsurface siliciclastic rocks of the São Francisco Craton, south-central Brazil: Precambrian Research, v. 103, p. 1–29, doi: 10.1016/S0301-9268(00)00071-1.

Souza, P.C. and Müller, G., 1984, Primeiras estruturas algais comprovadas na Formação Gandarela, Quadrilátero Ferrífero: Revista Escola de Minas, v. 37, p. 13–21.

Steiner, M. and Reitner, J., 2001, Evidence of organic structures in Ediacara-type fossils and associated microbial mats: Geology, v. 29, p. 1119–1122, doi: 10.1130/0091-7613(2001)029<1119:EOOSIE>2.0.CO.

Taj, R.J., Aref, M.A.M., and Schreiber, B.C., 2014, The influence of microbial mats on the formation of sand volcanoes and mounds in the Red Sea coastal plain, south Jeddah, Saudi Arabia: Sedimentary Geology, v. 311, p. 60–74, doi: 10.1016/j.sedgeo.2014.06.006.

Tavares, T.D., Martins, M. de S., Alkmim, F.F., and Lana, C., 2020, Detrital zircons from the Upper Três Marias Formation, São Francisco basin, SE Brazil: record of foreland deposition during the Cambrian?: Journal of South American Earth Sciences, v. 97, article 102395, doi: 10.1016/j.jsames.2019.102395.

Thomas, K., Herminghaus, S., Porada, H., and Goehring, L., 2013, Formation of Kinneyia via shear-induced instabilities in microbial mats: Philosophical Transactions of the Royal Society A: Mathematical, Physical and Engineering Sciences, v. 371, p. 1–19, doi: 10.1098/rsta.2012.0362.

Uhlein, G.J., Caxito, F.A., Frei, R., Uhlein, A., Sial, A.N., and Dantas, E.L., 2020, Microbially induced chromium isotope fractionation and trace elements behavior in lower Cambrian microbialites from the Jaíba Member, Bambuí Basin, Brazil: Geobiology, v. 19, p. 125–146, doi: 10.1111/gbi.12426.

Uhlein, G.J., Uhlein, A., Pereira, E., Caxito, F.A., Okubo, J., Warren, L.V., and Sial, A.N., 2019, Ediacaran paleoenvironmental changes recorded in the mixed carbonate-siliciclastic Bambuí Basin, Brazil: Palaeogeography, Palaeoclimatology, Palaeoecology, v. 517, p. 39–51, doi: 10.1016/j.palaeo.2018.12.022.

Vieira, L.C., Trindade, R.I.F.F., Nogueira, A.C.R.R., and Ader, M., 2007, Identification of a Sturtian cap carbonate in the Neoproterozoic Sete Lagoas carbonate platform, Bambuí Group, Brazil: Comptes Rendus-Geoscience, v. 339, p. 240–258, doi: 10.1016/j.srte.2007.02.003.

Visscher, P.T. and Stolz, J.F., 2005, Microbial mats as bioreactors: populations, processes, and products: Palaeogeography, Palaeoclimatology, Palaeoecology, v. 219, p. 87–100, doi: 10.1016/j.palaeo.2004.10.016.

Wang, Y., Wang, Y., and Du, W., 2017, A rare disc-like holdfast of the Ediacaran macroalga from South China: Journal of Paleontology, v. 91, p. 1091–1101, doi: 10.1017/jpa.2017.43.

Warren, L.V., Buatois, L.A., Mángano, M.G., Simões, M.G., Santos, M.G.M., Poiré, D.G., Riccomini, C., and Assine, M.L., 2020, Microbially induced pseudotraces from a Pantanal soda lake, Brazil: alternative interpretations for Ediacaran simple trails and their limits: Geology, v. 48, p. 857–861, doi: 10.1130/G47234.1.

Warren, L.V., Quaglio, F., Riccomini, C., Simões, M.G., Poiré, D.G., Strikis, N.M., Anelli, L.E., and Strikis, P.C., 2014, The puzzle assembled: Ediacaran guide fossil Cloudina reveals an old proto-Gondwana seaway: Geology, v. 42, p. 391–394, doi: 10.1130/G35304.1.

Xiao, S., Chen, Z., Zhou, C., and Yuan, X., 2019, Surfing in and on microbial mats: oxygen-related behavior of a terminal Ediacaran bilaterian animal: Geology, v. 47, p. 1054–1058, doi: 10.1130/G46474.1.

Xiao, S., Schiffbauer, J.D., McFadden, K.A., and Hunter, J., 2010, Petrographic and SIMS pyrite sulfur isotope analyses of Ediacaran chert nodules: implications for microbial processes in pyrite rim formation, silicification, and exceptional fossil preservation: Earth and Planetary Science Letters, v. 297, p. 481–495, doi: 10.1016/j.epsl.2010.07.001.

Ye, Q., Tong, J., Pang, K., Tian, L., Hu, J., and An, Z., 2020, Fossils or sedimentary structures? Carbonaceous spheroids from the shale of the Cryogenian Nantuo Formation in Shengnongjia area, South China: Precambrian Research, v. 345, article 105759, doi: 10.1016/j.precamres.2020.105759.

Zaine, M.F., 1991, Análise dos fósseis de parte da Faixa Paraguai (MS, MT) e seu contexto temporal e paleoambiental:Unpublished Ph.D. dissertation, Universidade de São Paulo, São Paulo, 218 p.

Zucatti Da Rosa, A.L., 2005, Evidências de vida no Ediacarano Inferior da Bacia do Itajaí, SC: Unpublished M.Sc. thesis, Universidade do Vale do Rio dos Sinos, São Leopoldo, 56 p.

Received 31 March 2022; accepted 10 February 2023.